

2018

# Synthesis of ionic liquids and magnetic ionic liquids and their application in dispersive liquid-liquid microextraction

Stephen Andrew Pierson  
*Iowa State University*

Follow this and additional works at: <https://lib.dr.iastate.edu/etd>

 Part of the [Analytical Chemistry Commons](#)

## Recommended Citation

Pierson, Stephen Andrew, "Synthesis of ionic liquids and magnetic ionic liquids and their application in dispersive liquid-liquid microextraction" (2018). *Graduate Theses and Dissertations*. 16437.  
<https://lib.dr.iastate.edu/etd/16437>

This Thesis is brought to you for free and open access by the Iowa State University Capstones, Theses and Dissertations at Iowa State University Digital Repository. It has been accepted for inclusion in Graduate Theses and Dissertations by an authorized administrator of Iowa State University Digital Repository. For more information, please contact [digirep@iastate.edu](mailto:digirep@iastate.edu).

**Synthesis of ionic liquids and magnetic ionic liquids and their application in  
dispersive liquid-liquid microextraction**

by

**Stephen A. Pierson**

A thesis submitted to the graduate faculty  
in partial fulfillment of the requirements for the degree of

MASTER OF SCIENCE

Major: Chemistry

Program of Study Committee:  
Jared L. Anderson, Major Professor  
Vincenzo Venditti  
Robbyn K. Anand

The student author, whose presentation of the scholarship herein was approved by the program of study committee, is solely responsible for the content of this thesis. The Graduate College will ensure this thesis is globally accessible and will not permit alterations after a degree is conferred.

Iowa State University

Ames, Iowa

2018

Copyright © Stephen Pierson, 2018. All rights reserved.

## TABLE OF CONTENTS

<b>ACKNOWLEDGMENTS</b> .....	iv
<b>ABSTRACT</b> .....	v
<b>CHAPTER 1 INTRODUCTION</b>	
1.1 Introduction to ionic liquids and microextraction techniques .....	1
1.2 Introduction to magnetic ionic liquids and their application in sample preparation .....	3
1.3 Organization of the thesis .....	4
References .....	5
 <b>CHAPTER 2 SYNTHESIS AND CHARACTERIZATION OF LOW VISCOSITY HEXAFLUOROACETYLACETONATE-BASED HYDROPHOBIC MAGNETIC IONIC LIQUIDS</b>	
Abstract .....	6
2.1 Introduction .....	7
2.2 Experimental .....	10
2.3 Results and Discussion .....	15
2.4 Conclusion .....	26
Acknowledgements .....	27
References .....	27
 <b>CHAPTER 3 RAPID ANALYSIS OF ULTRAVIOLET FILTERS USING IONIC LIQUID-BASED <i>IN SITU</i> DISPERSIVE LIQUID-LIQUID MICROEXTRACTION COUPLED TO HEADSPACE DESORPTION GAS CHROMATOGRAPHY-MASS SPECTROMETRY</b>	
Abstract .....	30
3.1 Introduction .....	31

3.2 Experimental .....	33
3.3 Results and Discussion .....	37
3.4 Conclusion .....	49
Acknowledgements .....	50
References .....	50
<b>CHAPTER 4 GENERAL CONCLUSIONS .....</b>	<b>53</b>
<b>APPENDIX A SUPPLEMENTAL INFORMATION ACCOMPANYING CHAPTER 2 .....</b>	<b>54</b>
<b>APPENDIX B SUPPLEMENTAL INFORMATION ACCOMPANYING CHAPTER 3 .....</b>	<b>60</b>

## ACKNOWLEDGEMENTS

First and foremost, I would like to thank my advisor Dr. Jared Anderson for giving me the opportunity to work in the laboratory and allowing me to express my creativity in my research. I would also like to thank him for his guidance and criticism as it has shaped me into a better scientist. I would also like to thank my committee members Dr. Robbyn Anand, and Dr. Vincenzo Venditti, for their guidance and support.

I would like to thank all of my former and current group members: Jiwoo An, Honglian Yu, Josias Merib, Cheng Zhang, Omprakash Nacham, Kevin Clark, He Nan, Jeff Purslow, Marcelino Varona, Ashley Bowers, Miranda Emaus, Gabriel Odugbesi, Chenghui Zhu, Qamar Farooq, along with all visiting professors and postdoctoral fellows: Drs. Cecilia Cagliero, Dongmei Lu, Kosuke Kuroda, Xi-Tian Peng, María José Trujillo-Rodríguez, Xiong Ding, and Deepak Chand for their support and help throughout the years.

I would also like to thank my parents Gloria and Wes Pierson for being supportive every step of the way. I would also like to give a special thanks to Jiwoo An and Jeff Purslow for being there for the good times and sticking by through all the hard times. I would not have made it through if it weren't for you. Lastly, I would like to thank my friends and the chemistry department faculty and staff at Iowa State.

**ABSTRACT**

Ionic liquids (ILs) have garnered much attention in the field of analytical chemistry as tunable solvents with a wide array of applications. Magnetic ionic liquids (MILs) are a subclass of ILs that contain a paramagnetic component in their structure. This paramagnetic feature allows for them to be manipulated by an external magnetic field, possibly reducing the need for centrifugation, which is both a time and labor-intensive process that many analytical extraction techniques involve. Preexisting MILs possess characteristics such as high viscosity and low hydrolytic stability, which are detrimental for their potential use in analytical applications. This thesis introduces design and synthesis of MILs with low viscosity and high hydrophobicity to expand their usability in dispersive liquid-liquid microextraction (DLLME) methods. Furthermore, ILs with varying structures were synthesized for their use in an in situ DLLME method coupled to headspace gas chromatography mass spectrometry (HS-GC-MS) for the rapid analysis of ultraviolet (UV) filters from real water samples. These studies highlight the versatility of ILs and MILs for their application in analytical techniques.

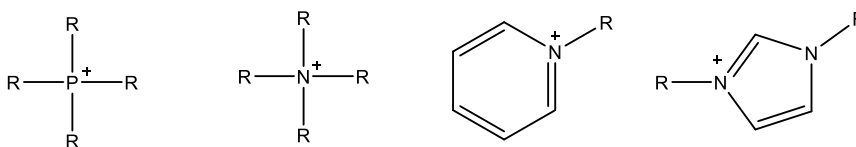
## CHAPTER 1

### INTRODUCTION

#### 1.1 Introduction to ionic liquids and their use in microextraction techniques

The continued development and understanding of ionic liquids (ILs) have opened a field of opportunity for many major disciplines of chemistry [1]. ILs are molten salts comprised of cations and anions with melting temperatures at or below 100 °C, possessing many favorable physicochemical properties such as low vapor pressure, high thermal stability, and high conductivity [2]. Their tunable structure gives them a distinct advantage over traditional organic solvents allowing for them to be tailored specifically towards a desired application [2, 3]. Some common IL cation and anion structures are shown in Figure 1.1.

#### Cations



#### Anions

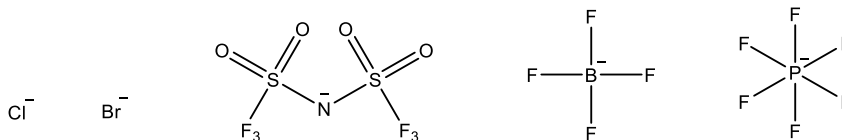


**Figure 1.1.** Common cations and anions used in ILs.

The use of ILs for sample preparation has been expanding rapidly over the last few decades [3]. Sample preparation is an essential part of the analytical process, which generally requires preconcentration and separation of target analytes from a complex matrix [4]. Traditional

procedures utilize techniques such as liquid-liquid extraction (LLE) and solid-phase extraction (SPE), which can be both time-consuming and labor-intensive. These techniques often utilize a large amount of harmful organic solvents. To overcome these drawbacks, much attention has been given to development of microextraction techniques.

Microextraction techniques can be classified into two main categories, solid-phase microextraction (SPME) and liquid-phase microextraction (LPME). SPME is a versatile technique in which a fiber is coated with a material, generally polymeric in nature, to be utilized as an extraction phase [5]. The non-exhaustive nature of the extraction process along with the reusability of the fibers employed are considered to be advantages of SPME. However, SPME methods generally call for long extraction times, which reduce the throughput of the method.

Liquid phase microextraction (LPME) techniques utilize small volumes of solvent to preconcentrate analytes from a sample matrix. Two examples of LPME are single drop microextraction (SDME) and dispersive liquid-liquid microextraction (DLLME). These LPME methods are widely used in industry because they are simple and inexpensive. In SDME, analytes partition into a small droplet of solvent (low  $\mu\text{L}$  scale volume) suspended from a syringe needle [6]. This technique can utilize both direct immersion and headspace sampling methods. Typically, long extraction times are needed for the analytes to reach an equilibrium between the sample matrix and the solvent droplet.

In DLLME, a mixture of extraction and disperser solvents are placed into a sample solution and dispersed into fine droplets by vortex or sonication [7]. Due to the high surface area of extraction phase created by dispersion, analytes undergo rapid equilibration with the extraction phase and sample matrix [8]. Traditionally, centrifugation is necessary to sediment and collect the extraction phase following extraction. The analyte-enriched extraction phase can be



directly injected into a gas chromatography (GC) or high-performance liquid chromatography (HPLC) instrument for analysis, or alternatively, analytes can be desorbed using high temperatures or a small amount of organic solvent prior to analysis. ILs can be utilized in LPME methods, conferring high selectivity by incorporation of desired functional groups into the IL structures. In *in situ* DLLME, an ion-exchange reagent is added along with an IL to an aqueous sample solution to create a hydrophobic IL that is immiscible with the aqueous phase [9]. This metathesis reaction and extraction are combined into one step, leading to fast and efficient preconcentration and sample clean up procedure.

## **1.2 Introduction to magnetic ionic liquids and their application in sample preparation**

Magnetic ionic liquids (MILs) are a sub class of ILs that incorporate a paramagnetic center into the cation or anion portion of the IL structure [10]. Incorporating this paramagnetic component can be advantageous in many sample preparation techniques. In DLLME procedures, the use of MILs allows collection of the extraction phase by introducing an external magnetic field without the need for centrifugation [11]. A comparison of traditional DLLME and MIL-based DLLME procedures are shown in Figure 1.2.

There are many challenges to creating MILs that are compatible with extraction techniques. Since many extractions utilize aqueous media, MILs are generally required to be extremely hydrophobic to prevent dissolution and or possible hydrolysis of the MIL. Further, the high viscosity of many MILs (or ILs) limits their application in sample preparation procedures. Existing hydrophobic MILs exhibit much higher viscosity when compared to some traditional ILs, leading to difficulties in utilizing MILs for techniques such as DLLME [10]. Therefore,

design of a new generation of MILs that possess low viscosity, high magnetic susceptibility and hydrophobicity is essential to expand their application in analytical chemistry.

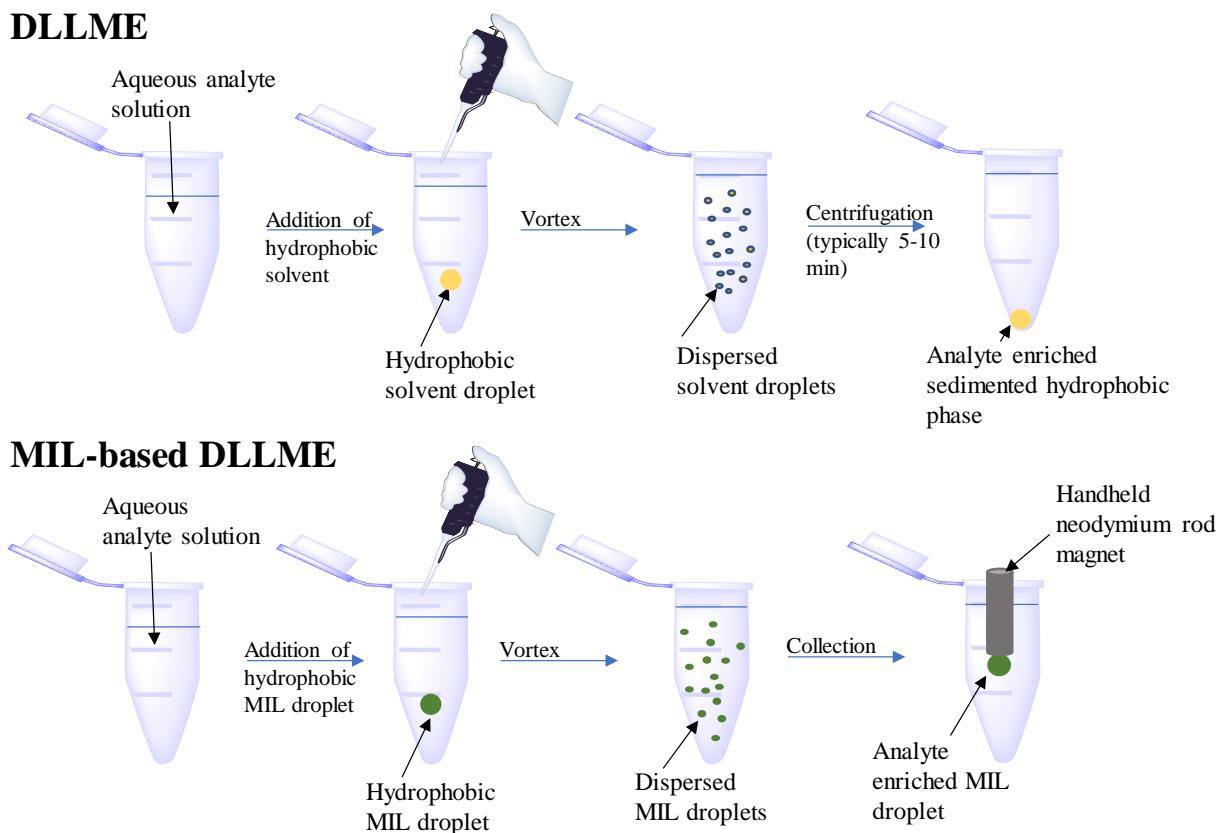


**Figure 1.2.** Schematic of conventional and MIL based DLLME procedures

### 1.3 Organization of the thesis

The main objectives of this thesis are to synthesize MILs suitable for analytical applications and to utilize traditional ILs in microextraction procedures paired with gas chromatography to monitor organic compounds. According to these main objectives, this thesis has been divided into the following chapters:

**Chapter 2** describes the synthesis and characterization of a new class of magnetic ionic liquids suitable for their use in analytical chemistry. The synthesized MILs are highly stable in

aqueous environments and have low viscosities making them attractive for techniques such as DLLME. Furthermore, high magnetic susceptibilities were achieved with the addition of rare earth metals dysprosium and gadolinium into the anion structure.

**Chapter 3** describes the development of an IL-based *in situ* DLLME extraction method in combination with headspace gas chromatography paired with mass spectrometry for the analysis of ultraviolet filters. The developed method allowed for rapid preconcentration of analytes into the IL extraction phase and was compatible with pool and lake water samples.

**Chapter 4** provides a short summary of the completed work.

## References

- [1] R.D. Rodgers, K.R. Seddon, *Science* 5646 (2003) 792
- [2] J.S. Wilkes, *Green Chem.* 4 (2002) 73
- [3] T.D. Ho, C. Zhang, L.W. Hantao, J.L. Anderson *Anal. Chem.* 86 (2013) 262
- [4] J. Pawliszyn, *Anal. Chem.* 75 (2003) 2543
- [5] J. Pawliszyn, *J. Chromatogr. Sci.* 38 (2000) 270
- [6] H. Liu, P.K. Dasgupta, *Anal. Chem.* 68 (1996) 1817
- [7] M. Rezaee, Y. Assadi, M.R. Milani Hosseini, E. Aghaee, F. Ahmadi, S. Berijani, *J. Chromatogr. A* 1116 (2006) 1
- [8] J. An, M.J. Trujillo-Rodriguez, V. Pino, J.L. Anderson, *J. Chromatogr. A* 1500 (2017) 1
- [9] C. Yao, J.L. Anderson, *Anal. Bioanal. Chem.* 395 (2009) 1491
- [10] K.D. Clark, O. Nacham, J.A. Purslow, S.A. Pierson, J.L. Anderson, *Anal. Chim. Acta* 934 (2016) 9
- [11] O. Nacham, K.D. Clark, J.L. Anderson, *RSC Adv.* 6 (2016) 11109

**CHAPTER 2****SYNTHESIS AND CHARACTERIZATION OF LOW VISCOSITY  
HEXAFLUOROACETYLACETONATE-BASED HYDROPHOBIC MAGNETIC  
IONIC LIQUIDS**

Reprinted with permission from *New Journal of Chemistry*, **2017**, 41, 5498-5505

Copyright © 2017, RSC

Stephen A. Pierson, Omprakash Nacham, Kevin D. Clark, He Nan, Yaroslav  
Mudryk, and Jared L. Anderson

**Abstract**

Magnetic ionic liquids (MILs) are distinguished from traditional ionic liquids (ILs) by the incorporation of a paramagnetic component within their chemical structure. Hydrophobic MILs are novel solvents that can be used in many applications, including liquid-liquid extraction (LLE) and catalysis. Low viscosity and low water solubility are essential features that determine their feasibility in LLE. In this study, extremely hydrophobic MILs were synthesized by using transition and rare earth metal hexafluoroacetylacetonate chelated anions paired with the trihexyl(tetradecyl)phosphonium ( $[P_{66614}^+]$ ) cation. Hydrophobic MILs exhibiting water solubilities less than 0.01% (v/v) were synthesized in a rapid two-step procedure. Furthermore, the viscosities of the MILs are among some of the lowest ever reported for hydrophobic MILs (276.5-927.9 centipoise (cP) at 23.7 °C) dramatically improving the ease of handling these liquids. For the first time, the magnetic properties of MILs possessing hexafluoroacetylacetonate chelated metal anions synthesized in this study are reported using a superconducting quantum interference device (SQUID) magnetometer. Effective magnetic moments ( $\mu_{\text{eff}}$ ) as high as 9.7 and 7.7 Bohr magnetons ( $\mu_B$ ) were achieved

by incorporating high spin dysprosium and gadolinium ions, respectively, into the anion component of the MIL. The low viscosity, high hydrophobicity, and large magnetic susceptibility of these MILs make them highly attractive and promising solvents for separations and purification, liquid electrochromic materials, catalytic studies, as well as microfluidic applications.

## 2.1 Introduction

Ionic liquids (ILs) have garnered much attention in the last decade due to an array of attractive physicochemical properties including negligible vapor pressure, high thermal stability, high conductivity, and tunable miscibility with water and organic solvents. These fascinating compounds are generally comprised of an organic cation paired with an organic/inorganic anion and possess melting points at or below 100 °C.<sup>1</sup> The physicochemical properties of ILs can be altered and tuned through the careful manipulation of cation/anion pairing making them highly versatile materials.<sup>2-7</sup>

Magnetic ionic liquids (MILs) are a subclass of ILs that share many of the advantageous physicochemical properties of traditional ILs.<sup>8-10</sup> MILs possess a paramagnetic metal center within the cation and/or anion that allow them to be modulated by an external magnetic field. The 1-butyl-3-methylimidazolium tetrachloroferrate(III) ([BMIM<sup>+</sup>][FeCl<sub>4</sub><sup>-</sup>]) MIL was the first example of an IL that incorporated a paramagnetic center in its chemical structure.<sup>8, 11</sup> Since then, a variety of transition and rare earth metals, such as Co(II), Mn(II), Fe(III), Dy(III), Gd(III), Ho(III), and Nd(III), have been used as paramagnetic centers in the preparation of MILs.<sup>12</sup>

MILs have enjoyed increasing popularity in applications such as liquid-liquid extractions (LLE), liquid-liquid microextractions (LLME), stationary phases for comprehensive two-dimensional gas chromatography ( $GC \times GC$ ), electrochemical applications, and catalysis.<sup>12-15</sup> The promising field of MILs is expanding rapidly, and thus the need for more robust, hydrophobic MILs has never been greater. Applications that utilize MILs as extraction solvents from aqueous environments require MILs that are extremely hydrophobic and chemically stable to retain their magnetic susceptibility and not suffer from dissolution or loss of the solvent.<sup>16</sup> Importantly, the magnetic susceptibility of MILs can only be exploited if they possess very little solubility in the solvent to which they are added (e.g., water). MILs that are room temperature liquids are required for applications performed at ambient temperatures. Therefore, MILs possessing high hydrophobicity, low melting points, low viscosity, as well as high magnetic susceptibility are all favorable properties when they are utilized as solvent systems in a number of applications (e.g., extractions and catalytic solvents).<sup>12-14</sup> Additionally, there is an underlying issue in MIL design that relates to the chemical stability of the MIL in an aqueous environment. Although it is a popular choice for the anion component of MILs, the  $[FeCl_4^-]$  anion has been shown to undergo hydrolysis in water thereby influencing solution pH and limiting the amount of MIL that can be recovered in applications involving water.<sup>18</sup> A design challenge revolves around creating MILs that encompass all of the aforementioned features with minimal compromise of any single feature.

The incorporation of hydrophobic trihexyl(tetradecyl)phosphonium ( $[P_{66614}^+]$ ) and Aliquat 336 cations has been a well-utilized strategy for creating hydrophobic ILs.<sup>12,19</sup> Furthermore, the weakly coordinating bis[(trifluoromethyl)sulfonyl]imide  $[NTf_2^-]$  anion has been used to increase the hydrophobicity as well as lower the viscosity for many classes of

ILs. However, MILs with  $[\text{NTf}_2^-]$  anions require either a multi-cationic platform with heteroanions or a paramagnetic component in the cation of the MIL to establish paramagnetic susceptibility. MILs utilizing the  $[\text{NTf}_2^-]$  anion in di- or tricationic frameworks involve tedious multistep synthetic pathways<sup>20-22</sup> while some MILs with paramagnetic cations have been shown to exhibit poor stability under ambient conditions. Alternatively, the hydrophobicity and viscosity of MILs can be significantly improved by pairing a hydrophobic cation with a weakly coordinating (hydrophobic) anion that can chelate with paramagnetic metal centers. In order to circumvent these challenges and produce hydrophobic ILs with low viscosity, hexafluoroacetylacetonate ( $[\text{hfacac}^-]$ ) metal chelates have been explored in which the bidentate ligand complexes with transition or rare earth metals by coordination of both  $[\text{hfacac}^-]$  oxygens to the metal center.<sup>23,24</sup>

In this study, a novel two-step synthesis was developed to create low melting, room temperature transition and rare earth metal-based MILs. Co(II), Mn(II), and Ni(II) metal centers were incorporated into the MIL structure to create trihexyl(tetradecyl)phosphonium tris(hexafluoroacetylaceto)cobaltate(II) ( $[\text{P}_{66614}^+]$   $[\text{Co(II)(hfacac)}_3^-]$ ),  $[\text{P}_{66614}^+]$  tris(hexafluoroacetylaceto)manganate(II) ( $[\text{Mn(II)(hfacac)}_3^-]$ ),  $[\text{P}_{66614}^+]$  tris(hexafluoroacetylaceto)nickelate(II) ( $[\text{Ni(II)(hfacac)}_3^-]$ ) MILs. Three rare earth metal centers dysprosium(III), gadolinium(III) and neodymium(III) were used to prepare  $[\text{P}_{66614}^+]$  tetrakis(hexafluoroacetylaceto)dysprosate(III) ( $[\text{Dy(III)(hfacac)}_4^-]$ ),  $[\text{P}_{66614}^+]$  tetrakis(hexafluoroacetylaceto)gadolate(III) ( $[\text{Gd(III)(hfacac)}_4^-]$ ), and  $[\text{P}_{66614}^+]$  tetrakis(hexafluoroacetylaceto)neodymate(III) ( $[\text{Nd(III)(hfacac)}_4^-]$ ) MILs. It was observed that all of the prepared MILs exhibited water solubilities less than 0.01% (v/v), making them ideal for MIL-based applications in aqueous systems. Furthermore, these MILs

were found to be soluble in nearly 15 organic solvents. Viscosities of the synthesized MILs ranged from 276.5 centipoise (cP) to 927.9 cP at 23.7 °C, making them among the least viscous hydrophobic MILs ever reported. Thermal properties of the MILs were investigated by monitoring the onset of volatilization/decomposition using flame ionization detection with thermal stabilities ranging from 130-225 °C. In addition, incorporation of Gd(III) and Dy(III) metal centers produced MILs with magnetic moments ( $\mu_{\text{eff}}$ ) of 7.7 and 9.7 Bohr magnetons ( $\mu_{\text{B}}$ ), respectively, as determined by SQUID magnetometry. This new class of MILs possess high hydrophobicity, low melting points, low viscosity, and high magnetic susceptibility making them ideal solvents for a number of applications ranging from catalysis to microfluidic applications where the MIL can be readily controlled and manipulated within the device.

## 2.2 Experimental

### 2.2.1 Materials

The reagents ammonium hydroxide (28-30% solution in water) and 1,1,1,5,5,5-hexafluoroacetylacetone (99%) were purchased from Acros Organics (Morris Plains, NJ, USA.) Gadolinium(III) chloride hexahydrate (99.9%) and manganese(II) chloride tetrahydrate (98.0-101.0%) were purchased from Alfa Aesar (Ward Hill, MA, USA.) Acetonitrile (99.9%), hexane (98.5%), methanol (99.9%), cobalt(II) chloride hexahydrate (98%), dysprosium(III) chloride hexahydrate (99.9%), nickel(II) chloride (98%), and neodymium(III) chloride hexahydrate were purchased from Sigma Aldrich (St. Louis, MO, USA). Anhydrous diethyl ether (99.0%) was purchased from Avantor Performance Materials Inc. (Center Valley, PA, USA). Ethanol (100%) was purchased from Decon Labs (King of



Prussia, PA, USA). Deuterated DMSO was obtained from Cambridge Isotope Laboratories (Andover, MA, USA.) All solvents and reagents were used as received without any additional drying or purification. Ultra-pure water (18.2 M $\Omega$  cm) was obtained from a Milli-Q water purification system (Millipore, Bedford, MA, USA). Trihexyl(tetradecyl)phosphonium chloride (>93%) was purchased from Strem Chemical (Newburyport, MA, USA). Trihexyl(tetradecyl)phosphonium chloride was further purified by dissolving 20 g of the IL in 50 mL of acetonitrile. The acetonitrile layer was washed three times with 5 mL aliquots of hexane. Acetonitrile was subsequently evaporated off under reduced pressure followed by drying of the IL at 50° C in a vacuum oven.

NMR spectra ( $^1\text{H}$ ) were recorded using a Bruker 500 MHz nuclear magnetic resonance spectrometer. Solvent peaks were used as reference values for the reporting of chemical shifts. Elemental analyses were obtained using a Perkin Elmer 2100 Series II CHN/S Analyzer (Waltham, MA, USA). Mass spectra were obtained using an Agilent 6230 TOF LC/MS (Santa Clara, CA, USA). Viscosity measurements were obtained using a Wells/Brookfield DV1 cone and plate viscometer using a CPA-51Z cone spindle. Each MIL was dried in a vacuum oven for 48 hours at 50 °C ensuring any water or residual solvents were completely removed from the MILs. Sample volumes of 0.5 mL were used for all MILs at a temperature (23.7 °C). Thermal stabilities of MILs **1-6** (see Table 2.1 and Scheme 2.1) were tested by examining the thermal volatilization/decomposition of the MIL when the MIL was used as a stationary phase in gas chromatography.<sup>34</sup> The MILs were coated onto a 3 m capillary column with a 0.28  $\mu\text{m}$  film thickness using the static coating method. The  $[\text{P}_{66614}^+][\text{Cl}^-]$  IL was also coated under the same conditions and was used as a reference. These tests were run using a

temperature program starting at 40 °C and increased at 1 °C/min to 350 °C on an Agilent 6850 gas chromatograph with a flame ionization detector (Santa Clara, CA, USA).

### 2.2.2 Preparation of transition metal-based MILs

MILs **1-3** were synthesized by dissolving 10 mmol of ammonium hydroxide in 30 mL of ethanol. The reaction vessel was then sealed with a rubber septum and 10 mmol of hexafluoroacetylacetone was added dropwise at a rate of approximately 1 mL/min to the reaction via syringe. A white vapor was allowed to settle before adding 3.3 mmol of cobalt(II) chloride hexahydrate. The reaction was allowed to stir at room temperature for 5 hours. The solvent was removed under reduced pressure and the crude product was redissolved in 20 mL of diethyl ether and washed several times with 5 mL aliquots of deionized water until the aqueous fraction yielded no precipitate during a  $\text{AgNO}_3$  test. Diethyl ether was evaporated and the anion was allowed to dry at 50°C overnight under reduced pressure. 1 mmol of the anion was added to 1 mmol of purified phosphonium chloride and dissolved in 30 mL of methanol. This reaction was allowed to stir overnight at room temperature. The solvent was evaporated and 20 mL of diethyl ether was added to dissolve the crude product. The ether layer was washed several times with 5 mL aliquots of deionized water until the aqueous fraction yielded no precipitate during a  $\text{AgNO}_3$  test. Ether was evaporated off and MIL **1** was dried at 50°C overnight under reduced pressure. For MILs **2** and **3**, the same procedure was followed using manganese(II) chloride tetrahydrate and nickel(II) chloride.

### 2.2.3 Preparation of rare earth-based MILs

MILs **4-6** were synthesized by dissolving 10 mmol of ammonium hydroxide in 30 mL of ethanol. The reaction vessel was then sealed with a rubber septum and 10 mmol of hexafluoroacetylacetone was added dropwise at a rate of approximately 1 mL/min to the

reaction via syringe. A white vapor was allowed to settle before adding 2.5 mmol of dysprosium(III) chloride hexahydrate. The reaction was allowed to stir at room temperature for 5 hours. The solvent was removed under reduced pressure and the crude product was redissolved in 20 mL of diethyl ether and washed several times with 5 mL aliquots of deionized water until the aqueous fraction yielded no precipitate during a  $\text{AgNO}_3$  test. Diethyl ether was evaporated and the anion was allowed to dry at  $50^\circ\text{C}$  overnight under reduced pressure. 1.2 mmol of the anion salt was added to 1 mmol of purified phosphonium chloride and dissolved in 30 mL of methanol. This reaction was allowed to stir overnight at room temperature. The solvent was evaporated and 10 mL of hexane was added to the crude product to precipitate out any unreacted anion salt and filtered off. Once more, the solvent was evaporated and 20 mL of diethyl ether was added to dissolve the crude product. The ether layer was washed several times with 5 mL aliquots of deionized water until the aqueous fraction yielded no precipitate during a  $\text{AgNO}_3$  test. Ether was evaporated off and MIL **4** was dried at  $50^\circ\text{C}$  overnight under reduced pressure. For MILs **5** and **6**, the same procedure was followed using gadolinium(III) chloride hexahydrate and neodymium(III) chloride hexahydrate.

#### 2.2.4 Characterization of Intermediates

1A. Red solid. Yield 82%. TOF LC/MS:  $m/z$  (-) 680.4.

2A. Yellow solid. Yield 79%. TOF LC/MS:  $m/z$  676.4.

3A. Green solid. Yield 81%. TOF LC/MS:  $m/z$  (-) 679.4.

4A. White solid. Yield 83%. TOF LC/MS:  $m/z$  (-) 992.7.

5A. White solid. Yield 82%. TOF LC/MS:  $m/z$  (-) 986.7.

6A. Pink solid. Yield 81%. TOF LC/MS:  $m/z$  (-) 972.6.

## 2.2.5 Characterization of MILs

### Characterization MIL 1

Dark red viscous liquid. Yield 92 %. Elem. anal. calcd (%)  $C_{47}H_{71}CoF_{18}O_6P$ : C, 48.50; H, 6.15; N, 0. Found: C, 49.09; H, 6.31; N, 0.03. TOF LC/MS: m/z (+) 483.4; (-) 680.4.

### Characterization MIL 2

Light orange viscous liquid. Yield 91 %. Elem. anal. calcd (%)  $C_{47}H_{71}MnF_{18}O_6P$ : C, 48.67; H, 6.17; N, 0. Found: C, 48.89; H, 6.22; N, 0.37. TOF LC/MS: m/z (+) 483.4; (-) 676.4.

### Characterization MIL 3

Dark green viscous liquid. Yield 90 %. Elem. anal. calcd (%)  $C_{47}H_{71}NiF_{18}O_6P$ : C, 48.51; H, 6.15; N, 0. Found: C, 48.72; H, 6.22; N, 0.27. TOF LC/MS: m/z (+) 483.4; (-) 679.4.

### Characterization MIL 4

Light gold viscous liquid. Yield 93 %. Elem. anal. calcd (%)  $C_{52}H_{72}DyF_{24}O_8P \cdot 2H_2O$ : C, 41.35; H, 5.07; N, 0. Found: C, 41.39; H, 4.74; N, 0.25. TOF LC/MS: m/z (+) 483.4; (-) 992.7.

### Characterization MIL 5

Light yellow viscous liquid. Yield 91 %. Elem. anal. calcd (%)  $C_{52}H_{72}GdF_{24}O_8P \cdot 2H_2O$ : C, 41.49; H, 5.09; N, 0. Found: C, 41.85; H, 4.67; N, 0.31. TOF LC/MS: m/z (+) 483.4; (-) 986.7.

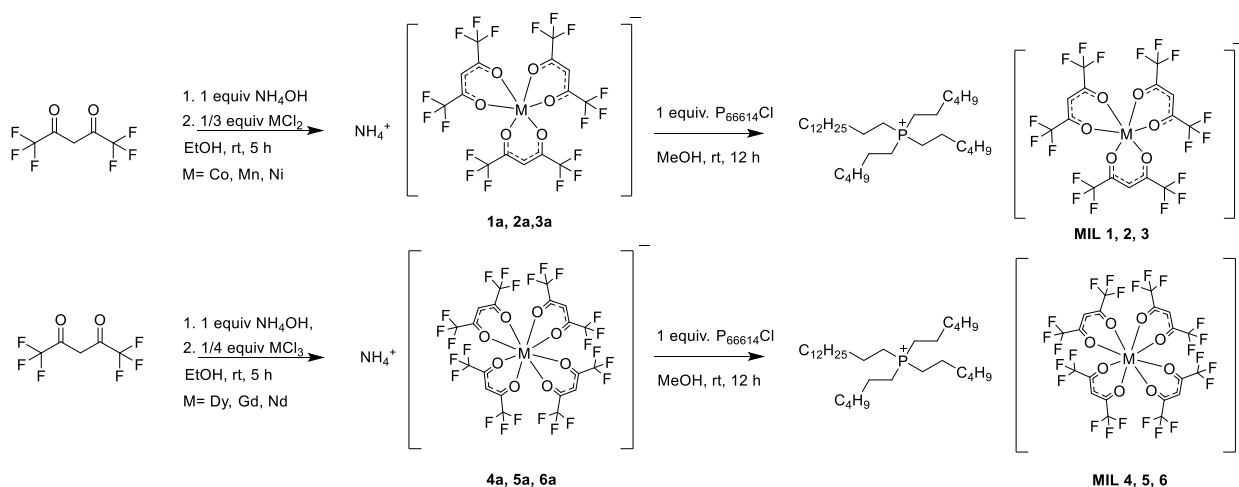
### Characterization MIL 6

Light pink viscous liquid. Yield 90 %. Elem. anal. calcd (%)  $C_{52}H_{72}NdF_{24}O_8P \cdot 2H_2O$ : C, 41.85; H, 5.13; N, 0. Found: C, 41.82; H, 4.53; N, 0.28. TOF LC/MS: m/z (+) 483.4; (-) 972.6.

## 2.3 Results and Discussion

### 2.3.1 Preparation and Evaluation of Hydrophobic MIL Structures.

ILs comprised of heavily alkylated phosphonium-based cations (i.e.,  $[P_{66614}^+]$ ) exhibit high hydrophobicity with relatively low melting points due largely to its asymmetry.<sup>27</sup> In addition, the  $[P_{66614}^+][Cl^-]$  IL is commercially available making the  $[P_{66614}^+]$  cation an attractive candidate for producing hydrophobic ILs. As shown in Scheme 2.1, reaction of ammonium hexafluoroacetylacetonate ( $[NH_4^+][hfacac^-]$ ) with various transition and rare earth metal centers yields the hydrophobic ammonium-based salt intermediates **1a-6a** that do not dissolve in water, even at very high ratios of water to salt. Pairing of intermediate **1a** to an imidazolium-based cation was carried out for preliminary viscosity and hydrophobicity testing. A metathesis reaction was performed between



Scheme 2.1. Synthesis of transition metal and rare earth-based magnetic ionic liquids

1-(6-hydroxyhexyl)-3-methylimidazolium chloride  $[MC_6OHIM^+][Cl^-]$  and intermediate **1a** to form  $[MC_6OHIM^+][Co(II)(hfacac)_3^-]$ . The resulting MIL was soluble in water as determined by an obvious color change in the aqueous solution two hours after addition of the MIL. Furthermore, the neat MIL could not be transferred with a pipette at room temperature due to

its high viscosity. Pairing the cation of the hydrophobic ammonium-based Aliquat 336 with intermediate **1a** also resulted in a very viscous MIL that could not be drawn into a pipette. Since the broad applicability of hydrophobic MILs is very much dependent upon the ease with which they can be transferred using traditional liquid handling methods, the  $[P_{66614}^+]$  cation was selected for preparation of the hfacac-based MILs.

Previously, transition metal hexafluoroacetylacetonate MILs were created in two different synthetic pathways, both involving a three-step synthesis.<sup>23,24</sup> In this study, the creation of metal salts **1a-6a** (Scheme 2.1) was achieved in a one-pot synthesis by reacting ammonium hydroxide, hexafluoroacetylacetonate, and the metal chloride salt. Reaction yields greater than 81% were achieved after 5 hours of total reaction time. It is important to highlight in this synthesis method the need to add hexafluoroacetylacetonate via syringe to the capped reaction vessel containing ethanol and ammonium hydroxide. The acid-base reaction between hexafluoroacetylacetonate and ammonium hydroxide causes a vapor to form inside the reaction vessel. Loss of this vapor resulted in low product yields <20%, presumably due to the vaporization of both hexafluoroacetylacetonate and ammonium hydroxide (which have boiling points <75 °C). The synthesis of the chelated metal salt was followed by a metathesis reaction between intermediates **1a-3a** and  $([P_{66614}^+][Cl^-])$ , thereby producing transition metal-based MILs **1-3** (Scheme 2.1) in a total of two steps.

The chelation of hexafluoroacetylacetonate to neodymium was also previously reported and although the crystal structure was isolated, the synthesis was limited by the solubility of the cation in the aqueous phase.<sup>23</sup> Furthermore, the reported procedure required reaction of the rare earth oxide  $NdO_3$  with bis(trifluoromethane)sulfonamide (HNTf<sub>2</sub>), an expensive reagent when compared to hexafluoroacetylacetonate. By eliminating the use of HNTf<sub>2</sub>, the cost of synthesis

of a 20 g batch of these rare earth-based MILs can be lowered from approximately \$380 to approximately \$90. To circumvent the limitations of this reaction, a synthesis similar to the transition metal analogues (Scheme 2.1) was followed to produce intermediates **4a-6a** after five hours in yields greater than 80%. A subsequent metathesis reaction between **4a-6a** and  $[P_{66614}^+][Cl^-]$  generated MILs **4-6** (Scheme 2.1). This synthetic strategy allows for the incorporation of rare earth metal centers possessing higher magnetic susceptibility, such as gadolinium and dysprosium, in a two-step synthesis.

The water solubility of these MILs was tested by pipetting a 1  $\mu$ L droplet of MIL into 10 mL of deionized water to create a 0.01% (v/v) solution. After pipetting the MIL into the aqueous sample, the MIL was observed to form a wide droplet that rests on top of the solution. Vortexing the MIL droplet caused dispersion of the MIL into fine microdroplets that were suspended within the aqueous solution, ultimately settling at the bottom of the vessel. The aqueous solution exhibited no observable change in color or pH, and the MIL droplets still responded readily to an external magnetic field after three days of suspension in the aqueous phase. These are all highly attractive features required in the design of low viscosity, hydrophobic MILs that possess high magnetic susceptibility. To demonstrate the hydrophobicity of these MILs compared to other available hydrophobic MILs, 50  $\mu$ L of  $[P_{66614}^+][FeCl_4^-]$ ,  $[P_{66614}^+][Co(II)(hfacac)_3^-]$ , and  $[P_{66614}^+][Nd(III)(hfacac)_4^-]$  were pipetted into separate scintillation vials containing 12 mL of deionized water. Each MIL was vortexed and heated to 85 °C for 10 minutes. Figure 2.1 shows a solution of the  $[P_{66614}^+][FeCl_4^-]$  MIL dissolving into the aqueous solution noted by discoloration while both  $[P_{66614}^+][Co(II)(hfacac)_3^-]$  and  $[P_{66614}^+][Nd(III)(hfacac)_4^-]$  MILs exhibit no sign of dissolution into the aqueous phase.

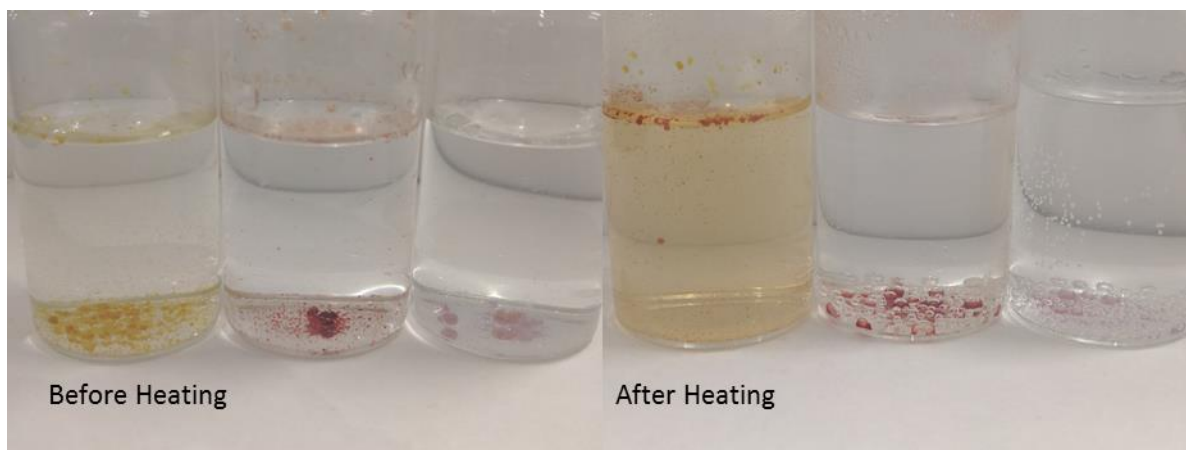


**Figure 2.1.**  $[P_{66614}^+][FeCl_4^-]$  (left),  $[P_{66614}^+][Co(II)(hfacac)_3^-]$  (middle), and  $[P_{66614}^+][Nd(III)(hfacac)_4^-]$  (right) before and after heating for 10 minutes at 85 °C.

The toxicity of the series of hydrophobic MILs was investigated using *Escherichia coli* (*E. coli*) as a model organism. After vortexing the bacteria in aqueous solution with each of the six studied hydrophobic MILs, no detectable differences in colony proliferation were observed for the Co(II), Mn(II), Ni(II), Dy(III), and Nd(III)-based MILs.<sup>25</sup> However, treatment with the  $[P_{66614}^+][Gd(III)(hfacac)_4^-]$  resulted in diminished growth of the bacteria indicating that the Gd(III)-based MIL possesses cytotoxicity toward *E. coli* K12 cells.

### 2.3.2 Solvent Miscibility

Owing to their unique solvation capabilities and high thermal stability, ILs have been successfully employed in organic synthesis either as reaction media or catalysts. An evaluation of the hydrophobic MIL solubility in a wide range of organic solvents may provide a fundamental understanding into their solvent properties. This could be instrumental for designing MIL-based reaction media, where the MIL can be selectively separated from the reaction products using an external magnetic field. The study was tested in 15 different organic solvents possessing a wide range of polarities. Table 2.1 shows the solubility of each MIL in



the different organic solvents. The transition-metal based MILs (MILs **1-3**) were fully miscible in all of the organic solvents except DMSO. A trend can be observed that the transition metal-based MILs show full miscibility in solvents with Reichardt's polarity index values<sup>26</sup> ranging from 0.117 (ethyl ether)-0.762 (methanol) at 20% (v/v) MIL to solvent ratio, with the exception of DMSO. However, as the polarity value of the solvent drops below 0.117, the transition-metal based MILs show decreased solubilities of 10% (v/v) MIL to solvent ratio. All of the transition metal-based MILs exhibited some solubility in DMSO, however, it was observed

**Table 2.1.** Physicochemical and Magnetic Properties of Transition and Rare Earth Metal-based MILs

MIL	Abbreviation	MW (g/mol)	Viscosity (cP) <sup>a</sup>	Solubility	$\mu_{\text{eff}}$ ( $\mu_{\text{B}}$ )
1	[P <sub>66614</sub> <sup>+</sup> ][Co(II)(hfacac) <sub>3</sub> <sup>-</sup> ]	1164.0	575.8	S <sup>b,c,e</sup>	4.3
2	[P <sub>66614</sub> <sup>+</sup> ][Mn(II)(hfacac) <sub>3</sub> <sup>-</sup> ]	1160.0	401.8	S <sup>b,c,e</sup>	5.8
3	[P <sub>66614</sub> <sup>+</sup> ][Ni(II)(hfacac) <sub>3</sub> <sup>-</sup> ]	1163.7	927.9	S <sup>b,c,e</sup>	2.8
4	[P <sub>66614</sub> <sup>+</sup> ][Dy(III)(hfacac) <sub>4</sub> <sup>-</sup> ]	1474.6	291.5	S <sup>c,d,e</sup>	9.7
5	[P <sub>66614</sub> <sup>+</sup> ][Gd(III)(hfacac) <sub>4</sub> <sup>-</sup> ]	1469.3	276.5	S <sup>c,d,e</sup>	7.7
6	[P <sub>66614</sub> <sup>+</sup> ][Nd(III)(hfacac) <sub>4</sub> <sup>-</sup> ]	1456.3	299.4	S <sup>c,d,e</sup>	2.8

<sup>a</sup>Viscosity measurements were performed at 23.7 °C. <sup>b</sup>Soluble in hexane, heptane, toluene, and benzene at 10% (v/v) MIL to solvent ratio. <sup>c</sup>Soluble in acetone, acetonitrile, chloroform, dichloromethane, dioxane, ethanol, ethyl acetate, diethyl ether, methanol, isopropyl alcohol at 20% (v/v) MIL to solvent ratio. <sup>d</sup>Soluble in hexane, heptane, toluene, and benzene at 20% (v/v) MIL to solvent ratio. <sup>e</sup>Insoluble in water at 0.01% (v/v) MIL to water ratio.  $\mu_{\text{eff}}$  = effective magnetic moment in Bohr magnetons ( $\mu_{\text{B}}$ ) determined from magnetic susceptibility data (from Quantum design SQUID magnetometer).

that fine droplets of insoluble MIL remain at a 10% (v/v) MIL to solvent ratio. The rare earth-based MILs were miscible in all of the tested solvents at 20% (v/v) MIL to solvent ratios. Furthermore, the rare earth-based MILs exhibit higher solubility in non-polar solvents such as benzene, toluene, heptane, and hexane when compared to the transition metal-based MILs. The lipophilicity of rare earth-based MILs is greater than that of the transition metal-based MILs due to an additional coordinated hexafluoroacetylacetonate ligand,<sup>27</sup> resulting in higher

solubility of the rare earth-based MILs in some non-polar solvents. The solubility of these MILs in many different organic solvents adds to their versatility and use in numerous applications.

### 2.3.3 Viscosity

Many previously synthesized hydrophobic MILs such as  $[P_{66614}^+]$  tetrachloromanganate(II) ( $[P_{66614}^+]_2[MnCl_4^{2-}]$ ),  $[P_{66614}^+]$  tetrachloroferrate(III) ( $[P_{66614}^+][FeCl_4^-]$ ), and  $[P_{66614}^+]$  hexachlorogadolate(III) ( $[P_{66614}^+]_3[GdCl_6^{3-}]$ ) possess high viscosities ranging from 650-83450 cP at 25 °C, which can be problematic when using them for a number of applications.<sup>12,29</sup> In this study, a strategy was implemented to lower the viscosity by creating a singly charged weakly coordinating metal anion paired with a cation that has previously been shown to produce MILs with low viscosity. The  $[P_{66614}^+][FeCl_4^-]$  MIL possesses a viscosity of 650 cP at 25 °C, which is much lower compared to the  $[P_{66614}^+]_2[MnCl_4^{2-}]$  (75230 cP at 25°C) and  $[P_{66614}^+]_3[GdCl_6^{3-}]$  (18390 cP at 25 °C) MILs.<sup>28</sup> The use of a  $\beta$ -diketonate ligand allows for an overall singly charged anion as well as high spin states for some of the metal centers. Viscosities of the MILs produced in this study are given in Table 2.1. The transition metal-based MILs all exhibit higher viscosities than the rare earth MILs, with the highest viscosity of 927 cP measured for the nickel-based MIL. An increasing trend of viscosities for the transition-metal MILs can be observed with a decrease in atomic radii from manganese to nickel (401.8 cP – 927.9 cP). As atomic radii of transition metals decrease, the metal-chelate bond distance also decreases,<sup>29</sup> reducing the overall size of the anion and increasing the strength of intermolecular forces and viscosity of these MILs.



**Figure 2.2.**  $[\text{P}_{66614}^+]_2[\text{MnCl}_4^{2-}]$  (left),  $[\text{P}_{66614}^+][\text{Ni(II)(hfacac)}_3^-]$  (middle), and  $[\text{P}_{66614}^+][\text{Nd(III)(hfacac)}_4^-]$  (right) before and after inversion for 1 second.

This trend in viscosity is also seen with other  $[\text{P}_{66614}^+]$  based magnetic ionic liquids with  $[\text{CoCl}_4^{2-}]$  and  $[\text{MnCl}_4^{2-}]$  anions.<sup>28</sup> The rare earth metal MILs possess exceedingly low viscosities at 23.7 °C (<300 cP) when compared to other  $[\text{P}_{66614}^+]$  based MILs such as  $[\text{P}_{66614}^+][\text{FeCl}_4^-]$  and  $[\text{P}_{66614}^+]_2[\text{MnCl}_4^{2-}]$ . The lower viscosity of rare-earth MILs compared to transition metal-based MILs can be attributed to the bulkier rare earth anions which create a less compact environment limiting intermolecular forces and reducing viscosity. Figure 2.2 compares the viscosities of  $[\text{P}_{66614}^+]_2[\text{MnCl}_4^{2-}]$ ,  $[\text{P}_{66614}^+][\text{Ni(II)(hfacac)}_3^-]$ , and  $[\text{P}_{66614}^+][\text{Nd(III)(hfacac)}_4^-]$  by performing a 1 second inversion of each MIL. The  $[\text{P}_{66614}^+]_2[\text{MnCl}_4^{2-}]$  MIL exhibits little to no movement down the vial due to its high viscosity while the  $[\text{P}_{66614}^+][\text{Ni(II)(hfacac)}_3^-]$  and  $[\text{P}_{66614}^+][\text{Nd(III)(hfacac)}_4^-]$  MILs flow easily toward the bottom of the vial. A visual comparison of viscosity of all MILs synthesized in this study as well as a side-by-side comparison of two different Mn-based MILs is demonstrated in Figures A12 and A13. It should also be noted that all of the studied hexafluoroacetylacetonate-based MILs could be easily pipetted at room temperature without heating.

### 2.3.4 Thermal Stability

The thermal stability of all MILs was tested using gas chromatography to reveal the onset temperature of volatilization/decomposition. To achieve this, an approximate 0.25-0.28  $\mu\text{m}$  film of IL/MIL was immobilized on the inner wall of a fused silica capillary.<sup>36</sup> The IL/MIL coated capillary was then heated slowly in a GC oven and an ultra-sensitive flame ionization detector (FID) was used to detect any volatilization/decomposition of the IL/MIL. Figure 2.3 shows the thermal stability diagram of each MIL as the temperature of the MIL within the capillary column is steadily increased. The reference column containing the  $[\text{P}_{66614}^+][\text{Cl}^-]$  IL produced the lowest thermal decomposition indicating that the presence of the metal anion complex limits the thermal stability of the MILs. The cobalt-based MIL showed the lowest thermal stability, with the onset of decomposition starting at approximately 130 °C and a sharp increase in the rate of decomposition occurring around 200 °C. The manganese-based MIL exhibited a similar profile with its degradation starting approximately 25 °C higher than the cobalt-based MIL. Conversely, the neodymium-based MIL showed the highest thermal stability out of all the MILs tested with slight and gradual degradation beginning around 225 °C. Gadolinium, dysprosium, and nickel-based MILs all exhibited similar thermal stabilities with more rapid decomposition of the MIL occurring above 215 °C.

### 2.3.5 Magnetic Susceptibility

MILs possess paramagnetic behavior that provides them distinct advantages over traditional ILs by allowing them to be easily removed or separated from an immiscible phase through the application of an external magnetic field. A handheld 1/16"  $\times$  1" neodymium-based rod magnet with a surface field of 6597 Gauss is sufficiently strong to collect small

droplets of MIL dispersed in aqueous media. A video demonstrating the MILs ability to be manipulated by an external magnetic field can be seen in the supplementary information.

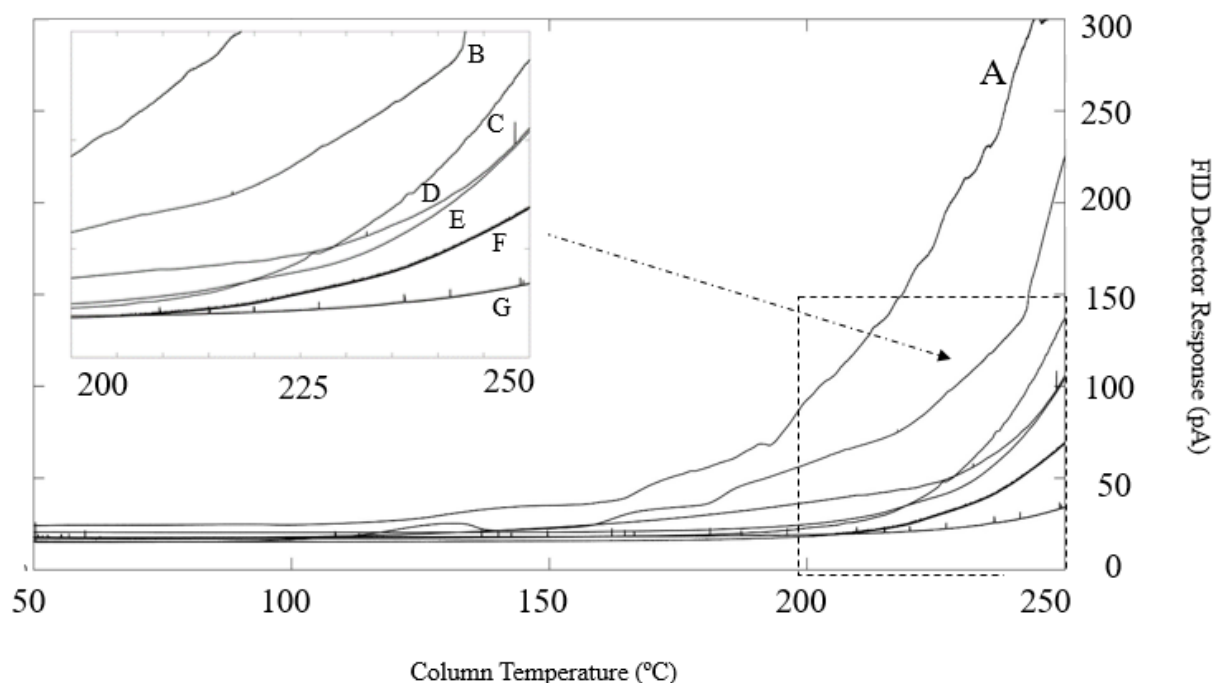


**Figure 2.3.** Thermal stability diagram constructed by coating a thin layer of MIL on the wall of fused silica capillary followed by heating under a constant flow of helium and detecting any volatilization/decomposition products using an ultra-sensitive flame ionization detector. A magnified inset from 200 to 250 °C is shown at the top left for clarity purposes. (A)  $[P_{66614}^+][Co(II)(hfacac)_3^-]$ ; (B)  $[P_{66614}^+][Mn(II)(hfacac)_3^-]$ ; (C)  $[P_{66614}^+][Gd(III)(hfacac)_4^-]$ ; (D)  $[P_{66614}^+][Dy(III)(hfacac)_4^-]$ ; (E)  $[P_{66614}^+][Ni(II)(hfacac)_3^-]$  (F)  $[P_{66614}^+][Nd(III)(hfacac)_4^-]$ ; (G)  $[P_{66614}^+][Cl^-]$ .

Octahedral complexes of Co(II), Mn(II), and Ni(II) all exhibit paramagnetism at room temperature.<sup>30-32</sup> Likewise, the rare earth metals Dy(III), Gd(III), and Nd(III) with eight coordinating species have also shown paramagnetism at ambient temperatures.<sup>33,34</sup> Exposure to a magnetic field results in spin alignment of unpaired electrons in the 3d orbital for the transition metal MILs and the 4f orbital for rare earth MILs. Removal of the magnetic field results in random spin orientation due to thermal motion, which creates a loss of magnetization.

Most paramagnetic materials exhibit an inverse relationship between magnetic susceptibility and temperature as defined by the Curie-Weiss law.

The  $\mu_{\text{eff}}$  values for each MIL were determined using a Quantum Design MPMS SQUID magnetometer following procedures similar to those previously reported.<sup>35</sup> Figure 2.4(a) shows the temperature dependence of magnetization for the  $[\text{P}_{66614}^+][\text{Co(II)(hfacac)}_3^-]$  MIL. Figure 2.4(b) shows a plot representing the linear portion of the reciprocal susceptibility versus temperature diagram for the octahedrally coordinated cobalt MIL. The calculated  $\mu_{\text{eff}}$  for the  $[\text{P}_{66614}^+][\text{Co(II)(hfacac)}_3^-]$  MIL was  $4.3 \mu_{\text{B}}$ , which agrees with previously reported literature values for high spin state Co(II) complexes.<sup>30,32</sup> The nickel-based MIL exhibits a  $\mu_{\text{eff}}$  of  $2.8 \mu_{\text{B}}$  at lower temperatures, also in agreement with literature values, but displays an anomaly in the temperature versus reciprocal mass susceptibility plot. This is presumably due to a phase transition of the MIL from a solid to liquid at approximately 150 K.<sup>30</sup> The octahedrally coordinated  $[\text{P}_{66614}^+][\text{Mn(II)(hfacac)}_3^-]$  possesses a high-spin  $d_5$  manganese(II) metal center and exhibits a  $\mu_{\text{eff}}$  of  $5.8 \mu_{\text{B}}$  at lower temperatures which agrees with literature reports, but is slightly lower ( $5.5 \mu_{\text{B}}$ ) at higher temperatures.<sup>31,32</sup> Plots for nickel and manganese-based MILs are lower ( $5.5 \mu_{\text{B}}$ ) at higher temperatures.<sup>31,32</sup> Plots for nickel and manganese-based MILs are represented by Figures A1 and A2 found in the supplemental information.

MILs exhibiting higher magnetic susceptibility were achieved by chelating rare earth gadolinium(III) and dysprosium(III) ions possessing high magnetic moments into the anion structure. Figure 2.5(a) shows the temperature dependence of magnetization for  $[\text{P}_{66614}^+][\text{Dy(III)(hfacac)}_4^-]$ . The plot of reciprocal susceptibility versus temperature is illustrated in Figure 2.5(b) and shows good linearity. Plots of reciprocal susceptibility versus

temperature for  $[P_{66614}^+][Gd(III)(hfacac)_4^-]$  and  $[P_{66614}^+][Nd(III)(hfacac)_4^-]$  also show good linearity at temperatures up to 250 K as illustrated in Figures A3 and A4.

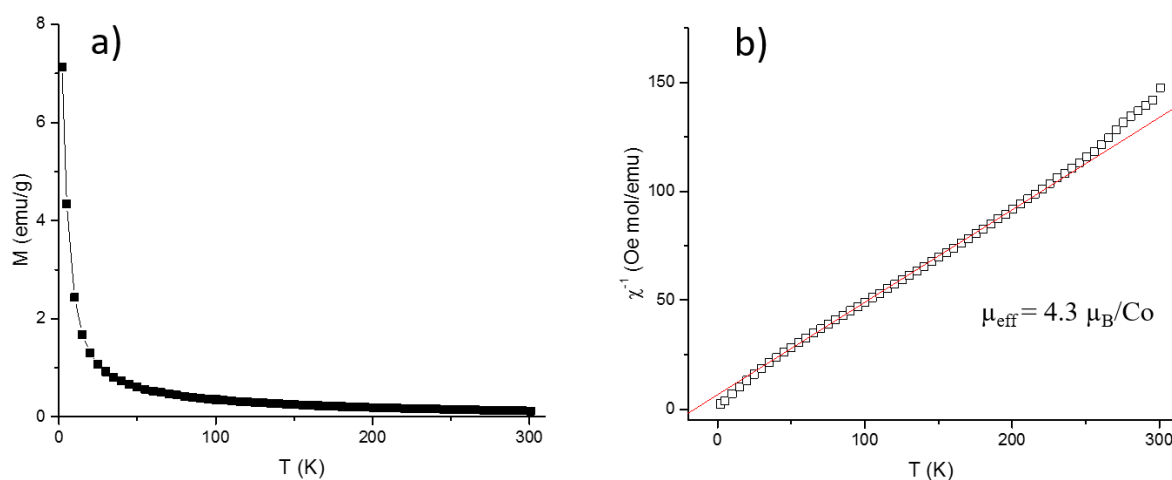


**Figure 2.4.** (a) Magnetization of the the  $[P_{66614}^+][Co(II)(hfacac)_3^-]$  MIL measured as a function of temperature in a 20000 Oe applied magnetic field (b) Curie-Weiss fit of the linear portion of the reciprocal susceptibility.

The  $\mu_{\text{eff}}$  of the dysprosium, gadolinium, and neodymium-based MILs were  $9.7 \mu_B$ ,  $7.7 \mu_B$ , and  $2.8 \mu_B$ , respectively, which are in accordance with previously reported eight coordinate dysprosium, gadolinium, and neodymium complexes.<sup>33,34</sup> When collecting fine droplets of dispersed dysprosium and gadolinium-based MILs, they can be observed to coalesce onto a rod magnet more easily compared to MILs with lower  $\mu_{\text{eff}}$ , including the neodymium and nickel-based MILs. However, all MILs synthesized in this study respond sufficiently to a handheld rod magnet allowing for their removal from aqueous solution.

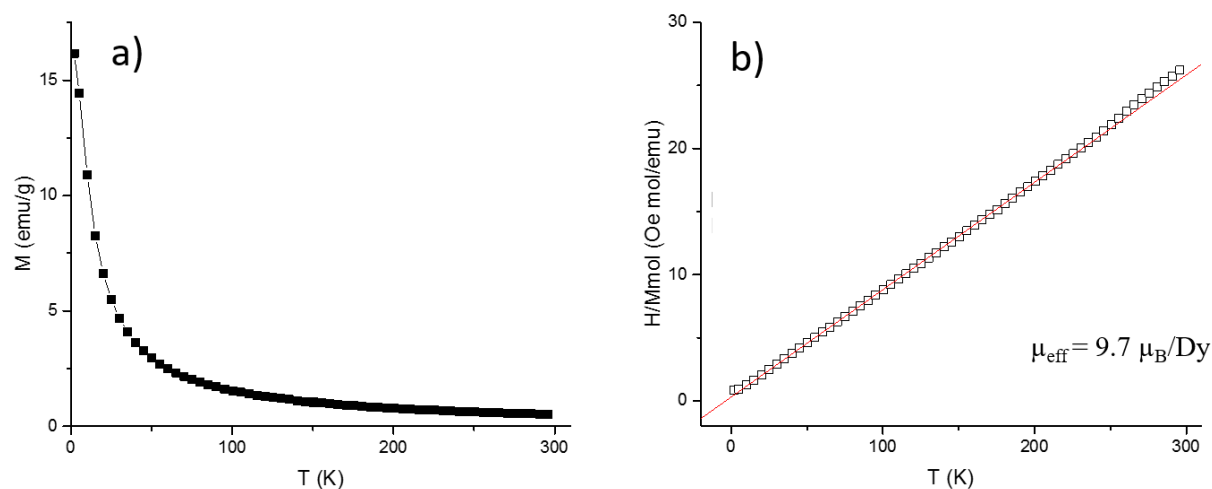


**Figure 2.5.** (a) Magnetization of the  $[P_{66614}^+][Dy(III)(hfacac)_4^-]$  MIL measured as a function of temperature in a 20000 Oe applied magnetic field (b) Curie-Weiss fit of the linear portion of the reciprocal susceptibility.

## 2.4 Conclusions

In this study, transition and rare earth metal-based MILs were successfully prepared in a two-step synthesis. Pairing of the  $[P_{66614}^+]$  cation and hexafluoroacetylacetonate chelated metal anions produced extremely hydrophobic MILs that were insoluble in aqueous solution at 0.01% (v/v). Furthermore, these MILs were miscible in a variety of polar and non-polar organic solvents. The neat hydrophobic MILs exhibited low viscosities ranging from 276.5- 927.9 cP at 23.7 °C. Moreover, increased magnetic susceptibility was achieved through the addition of high spin rare earth dysprosium and gadolinium ions into the anion structure yielding MILs with magnetic susceptibilities of 9.7 and 7.7  $\mu_B$ , respectively. Overall these MILs possess unique characteristics that can have great potential uses in various chemical applications such as extraction solvents in LLE, liquid electrochromic materials (Co-based MILs), and novel reaction media for organic synthesis.



## Acknowledgements

The authors acknowledge funding from the Chemical Measurement and Imaging Program at the National Science Foundation (Grant number CHE-1413199). The magnetic susceptibility measurements (Y.M.) were performed at Ames Laboratory (work supported by the Department of Energy, Office of Basic Energy Sciences, Materials Sciences Division). The Ames Laboratory is operated for the U. S. Department of Energy by Iowa State University of Science and Technology under contract No. DE-AC02-07CH11358.

## References

- [1] J. P. Hallett, T. Welton, *Chem. Rev.* 111 (2011) 3508
- [2] J. J. H. Davis, *Chem. Lett.* 33 (2004) 1072
- [3] F. Endres, S. Zein El Abedin, *Phys. Chem. Chem. Phys.* 8 (2006) 2101
- [4] S.T. Handy, *Curr. Org. Chem.* 9 (2005) 959
- [5] S. Sowmiah, V. Srinivasadesikan, M. C. Tseng, Y. H. Chu, *Molecules* 14 (2009) 3780
- [6] D. Rooney, J. Jacquemin, R. Gardas, *Ionic Liquids*, Berlin/Heidelberg: Springer (2009) 185
- [7] W. H. Awad, J. W. Gilman, M. Nyden, R. H. Harris, T. E. Sutto, J. Callahan, P. C. Trulove, H. C. DeLong, D. M. Fox, *Thermochimic. Acta* 409 (2004) 3
- [8] S. Hayashi, H. Hamaguchi, *Chem. Lett.* 33 (2004) 1590
- [9] Y. Yoshida, G. J. Saito, *Phys. Chem. Chem. Phys.* 12 (2010) 1675
- [10] T. Inagaki, T. Mochida, *Chem. Lett.* 39 (2010) 572
- [11] M. S. Sitze, E. R. Schreiter, E. V. Patterson, R. G. Freeman, *Inorg. Chem.* 40 (2001) 2298

- [12] K. D. Clark, O. Nacham, J. A. Purslow, S. A. Pierson, J. L. Anderson, *Anal. Chim. Acta* 934 (2016) 9
- [13] E. Santos, J. Albo A. Irabien, *RSC Adv.* 4 (2014) 40008.
- [14] A. Joseph, G. Żyła, V. I. Thomas, P. R. Nair, A. S. Padmanabhan, S. Mathew, *J. Mol. Liq.* 218 (2016) 319
- [15] H. Wang, R. Yan, Z. Li, X. Zhang, S. Zhang, *Catal. Commun.* 11 (2010) 763-767.
- [16] K. D. Clark, O. Nacham, H. Yu, T. Li, M. M. Yamsek, D. R. Ronning, J. L. Anderson, *Anal. Chem.* 87 (2015) 1552
- [17] K. D. Clark, M. M. Yamsek, O. Nacham, J. L. Anderson, *Chem. Commun.* 51 (2015) 16771
- [18] Z. L. Xie, A. Taubert, *ChemPhyschem* 12 (2011) 364
- [19] R. E. Del Sesto, T. M. McCleskey, A. K. Burrell, G. A. Baker, J. D. Thompson, B. L. Scott, J. S. Wilkes, P. Williams, *Chem. Commun.* 0 (2008) 447
- [20] O. Nacham, K. D. Clark, H. Yu, J. L. Anderson, *Chem. Mater.* 27 (2015) 923
- [21] Y. Yoshida, G. Saito, *J. Mater. Chem.* 16, (2006) 1254
- [22] O. Nacham, K. D. Clark, J. L. Anderson, *RSC Adv.* 6 (2016) 11109
- [23] H. Mehdi, K. Binnemans, K. Van Hecke, L. Van Meervelt, P. Nockemann, *Chem. Commun.* 46 (2010) 234
- [24] P. Zhang, Y. Gong, Y. Lv, Y. Guo, Y. Wang, C. Wang, H. Li, *Chem. Commun.* 48 (2012) 2334
- [25] K. D. Clark, J. A. Purslow, S. A. Pierson, O. Nacham, J. L. Anderson, *Anal. Bioanal. Chem.* 409 (2017) 4983
- [26] C. Reichardt, *Chem. Rev.* 94 (1994) 2319
- [27] Q. Lui, L. Xue, G. Zhao, *Synth. React. Inorg. Met.-Org. Chem.* 46 (2016) 888
- [28] E. Santos, J. Albo, A. Rosatella, C. A. M. Afonso, Á. Irabien, *J. Chem. Technol. Biotechnol.* 89 (2014) 866
- [29] R.F. See, R.A. Kruse, W.M. Strub, *Inorg. Chem.* 37 (1998) 5369

- [30] F. H. Field, W. C. Vosburgh, *J. Am. Chem. Soc.* 71 (1949) 2398
- [31] R. van Gorkum, F. Buda, H. Kooijman, A. L. Spek, E. Bouwman, J. Reedijk, *Eur. J. Inorg. Chem.* 11 (2005) 2255
- [32] N. Raman, S. Ravichandran, C. J. Thangaraja, *Chem. Sci.* 116 (2004) 215
- [33] B. Mallick, B. Balke, C. Felser, A. V. Mudring, *Angew. Chem. Int. Ed.* 47 (2008) 7635
- [34] K. Binnemans, Y. G. Galymetdinov, R. Van Deun, D. W. Bruce, S. R. Collinson, P. Polishchuk, I. Bikchantaev, W. Haase, A. V. Prosvirin, L. Tinchurina, I. Litvinov, A. Gubajdullin, A. Rakhmatullin, K. Uyttendhoeven, L Van Meervelt, *J. Am. Chem. Soc.* 122 (2000) 4335
- [35] Y. Mudryk, P. Manfrinetti, V. Smetana, J. Liu, M. L. Fornasini, A. Provino, V. K. Pecharsky, G. J. Miller, K. A. Gschneidner, *J. Alloys Compd.* 557 (2013) 252
- [36] C. F. Poole, *The Essence of Chromatography*. Elsevier Science (2003)

## CHAPTER 3

**RAPID ANALYSIS OF ULTRAVIOLET FILTERS USING IONIC LIQUID-BASED  
*IN SITU* DISPERSIVE LIQUID-LIQUID MICROEXTRACTION COUPLED TO  
HEADSPACE DESORPTION GAS CHROMATOGRAPHY-MASS  
SPECTROMETRY**

Stephen A. Pierson, María J. Trujillo-Rodríguez, Jared L. Anderson\*

**Abstract**

An ionic liquid (IL)-based *in situ* dispersive liquid-liquid microextraction (DLLME) method coupled to headspace desorption gas chromatography-mass spectrometry (HS-GC-MS) was developed for the rapid analysis of ultraviolet (UV) filters. The chemical structures of five ILs were specifically designed to incorporate various functional groups for favorable extraction of the target analytes. Extraction parameters including IL mass, molar ratio of IL to metathesis reagent, vortex time, ionic strength, pH, and total sample volume were studied and optimized. The effect of the headspace temperature and volume during the headspace desorption step was also evaluated to increase the sensitivity of the method. The optimized *in situ* DLLME procedure is fast as it only requires ~7–10 min per extraction and allows for multiple extractions to be performed simultaneously. In addition, the method exhibited high precision, good linearity, and low limits of detection for the six UV filters in aqueous samples. The developed method was also applied to both pool and lake water samples attaining acceptable relative recovery values.

### 3.1 Introduction

Skin cancer has become an increasing threat with the ongoing depletion of the Earth's ozone layer resulting in more ultraviolet (UV) radiation making it down to the earth's surface [1]. To combat this, UV filters have been used for decades as ingredients within a variety of products such as sunscreens, makeup, and other topical creams. UV filters are organic molecules that contain various functional groups that can absorb harmful UV radiation from the sun, thereby protecting the dermal layer of skin from being harmed by high energy UV-B and UV-C light [2, 3]. UV filters are also employed to protect plastics, paints, and other products from degradation due to UV exposure [4].

With the widespread use of UV filters in both plastics and topical protection, they can accumulate in different aquatic environments, especially swimming pools, lakes, and oceans [1, 2, 5]. Despite their benefits, recent reports have shown that UV filters can also have some negative effects on human and environmental health [5, 6]. Environmental agencies within the European Union (EU) have begun to regulate the presence of one of these compounds, 2-ethylhexyl methoxycinnamate (EMC), with other similar compounds likely to be regulated in the near future [7]. Therefore, the development of methods suitable for the extraction and detection of UV filters at low concentration levels is necessary.

High-performance liquid chromatography (HPLC) and gas chromatography (GC) coupled with mass spectrometry (MS) have been employed in a number of methods to analyze these analytes from real samples [3, 5, 7-14]. A variety of sample preparation techniques have been exploited prior to chromatographic separation for the extraction and preconcentration of these analytes. Traditionally, solid-phase extraction (SPE) has been the analytical method of choice for the extraction of EMC [2]. However, SPE techniques require large volumes of sample and

organic solvents. In recent years, there has been a push towards the development of automated sample preparation methods that require only small amounts of solvents and sample [15]. Fitting these criteria, solid-phase microextraction (SPME) and stir bar sorptive-dispersion microextraction (SBSD $\mu$ E) methods have been used for the extraction of UV filters [2, 4, 10, 16-18]. However, these techniques often require long extraction times and cleaning steps after extraction that can lead to lower throughput analysis. Liquid phase microextraction (LPME) has also been utilized for the extraction of UV filters from aqueous samples. LPME techniques include dispersive liquid-liquid microextraction (DLLME) [3, 11, 19], single drop microextraction (SDME) [1, 20] and hollow-fiber liquid phase microextraction (HF-LPME) [21].

Ionic liquids (ILs) have been explored as alternative solvents in LPME, as some classes of ILs may reduce toxic waste generation and contribute to an environmentally-friendly methodology [15, 22]. ILs are molten salts that possess melting points at or below 100 °C, tunable viscosities, negligible vapor pressure, and high thermal stability [23]. ILs have been utilized in SDME and HF-LPME for the determination of UV filters. However, these techniques generally require long extraction times. In an effort to increase sample throughput while achieving modest enrichment factors, IL-based DLLME techniques have gained popularity. *In-situ* IL-DLLME is a technique in which a hydrophilic IL is added to the aqueous sample, followed by the addition of a metathesis reagent [24, 25]. This mixture facilitates the *in-situ* formation of a hydrophobic IL in which analytes are preconcentrated. The *in-situ* approach forms large amounts of hydrophobic IL microdroplets which greatly increase the surface area of the extraction phase. The enhanced surface area achieved by *in-situ* DLLME has been shown to be more effective at extracting analytes compared to traditional DLLME

approaches [24-26]. Furthermore, the chemical structures of ILs can be tailored with different functional groups in order to facilitate different interactions with the analytes and achieve high extraction efficiency. The low vapor pressure of ILs allows them to be heated at high temperatures with little to no background interference, a property that can be exploited for headspace (HS)-GC-MS applications [17, 27, 28]. For the extraction of semi-volatile analytes such as UV filters, higher temperatures can result in increased sensitivity in HS-GS-MS analyses [27, 29-31].

In this study, five ILs have been specifically designed with different functional groups i.e., (long alkyl chains, aromatic moieties, and hydroxyl groups) to promote  $\pi$ - $\pi$ , hydrophobic, and hydrogen bonding interactions with 8 UV filters. Rapid preconcentration of UV filters was achieved using *in-situ* DLLME followed by analysis using HS-GC-MS. Extraction parameters including HS temperature and sampling volume, droplet size after *in situ* DLLME, total extraction volume, molar ratio of IL to metathesis reagent, ionic strength, pH and vortex time during the *in situ* DLLME were all optimized in this study.

## 3.2 Experimental

### 3.2.1 Materials

The analytes 2-ethylhexyl salicylate (ES; 99%), benzyl salicylate (BS; 99%), homosalate (HS; pharmaceutical secondary standard), oxybenzone (BP3; pharmaceutical secondary standard), menthyl anthranilate (MA; 98%), ethyl 2-cyano-3, 3 diphenyl-acrylate (ETO; 98%), 2-ethylhexyl 4-(dimethylamino)benzoate (EPP; 98%), and 2-ethylhexyl 4-methoxycinnamate (EMC; 98%) were purchased from Sigma-Aldrich (St. Louis, MO, USA). Individual standard

stock solutions were prepared by dissolving each analyte in acetone at a concentration of 2 mg mL<sup>-1</sup>.

The reagents 1-methylimidazole (99%), 1-benzylimidazole (99%), 1-bromobutane (99%), 2-bromoethanol (95%), 1-bromooctane (99%), 6-chlorohexanol (96%), acetone (99.5%), chloroform (99.5%), 2-propanol (99.5%), and acetonitrile (99.5%) were purchased from Sigma-Aldrich (St. Louis, MO, USA). Natural polypropylene conical centrifuge tubes (5 mL) were purchased from Sigma-Aldrich. Round bottom polystyrene centrifuge tubes (14 mL) and 3 mm diameter economical solid glass beads (Walter Stern) were purchased from Fisher Scientific (Fair Lawn, NJ, USA). Lithium bis[(trifluoromethyl)sulfonyl]imide (LiNTf<sub>2</sub>) was purchased from SynQuest Labs, Inc. (Alachua, FL, USA). Ultrapure water (18.2 M cm) was obtained from a Milli-Q water purification system (Bedford, MA, USA). Headspace vials (10 mL) and crimped silver aluminum caps with PTFE/silicone septum were purchased from Agilent Technologies (Santa Clara, CA, USA).

### 3.2.2 Synthesis of Ionic Liquids

The following five ILs were designed and synthesized in this study: 1-butyl-3-methylimidazolium bromide ([BMIM<sup>+</sup>][Br<sup>-</sup>]), 1-octyl-3-methylimidazolium bromide ([OMIM<sup>+</sup>][Br<sup>-</sup>]), 1-benzyl-3-butylimidazolium bromide ([BeBIM<sup>+</sup>][Br<sup>-</sup>]), 1-(6-hydroxyhexyl)-3-methylimidazolium chloride ([HeOHMIM<sup>+</sup>][Cl<sup>-</sup>]), and 1-benzyl-3-(2-hydroxyethyl)imidazolium bromide ([BeEOHIM<sup>+</sup>][Br<sup>-</sup>]). The structures of each IL are shown in Table 3.1. All ILs were synthesized according to previously reported literature procedures [24, 27, 32] and were characterized by <sup>1</sup>H NMR. <sup>1</sup>H NMR spectra for all ILs are shown in Fig. B1-B5 (Appendix B) and were recorded in deuterated chloroform or dimethyl sulfoxide using



a Bruker DRX 500 MHz nuclear magnetic resonance (NMR) spectrometer (Billerica MA, USA).

### 3.2.3 Instrumentation

An Agilent 7890B gas chromatograph (Santa Clara, CA, USA) equipped with a 5977A mass spectrometer and an Agilent 7697A headspace sampler was used for the HS-GC-MS analysis of the 8 UV filters. The HS sampler was operated in fill mode (flow to pressure, 50 psi) with the HS oven operating at an optimized temperature of 200 °C. The sample loop and transfer line were maintained at 210 °C and 220 °C, respectively. An equilibration time of 10 min with no agitation was used for all experiments. The GC injector was maintained at 250 °C with a 5:1 split ratio. Separations were achieved using an HP-5MS UI capillary column (30 m × 250 µm I.D., 0.25 µm film thickness) obtained from Agilent Technologies. Helium was used as the carrier gas at constant flow of 1 mL·min<sup>-1</sup>. The temperature program used was as follows: initial temperature was set at 100 °C (held for 1 min) followed by a ramp from 100 °C to 290 °C at 25 °C min<sup>-1</sup> (held for 5 min). The transfer line was kept at 250 °C. The MS was operated in electron ionization mode (EI) at 70 eV, using 230 °C and 150 °C as source and quadrupole temperatures, respectively. Data were initially acquired in SCAN mode to determine the retention time of each of the 8 analytes. For subsequent analyses, the single ion monitoring (SIM) acquisition mode was used for detection/quantitation. Retention times, target and qualifier ions, and the segment program used for SIM mode are shown in Table B1.

### 3.2.4 In-situ dispersive liquid-liquid microextraction procedure

A working solution of UV filters was prepared at a concentration of 200 µg L<sup>-1</sup> for ES, BS, HS, BP3, MA, EMC and 1 mg L<sup>-1</sup> for ETO and EPP. To conduct a comparison of extraction efficiencies using the different ILs, a 5 mL conical centrifuge tube was filled with 4.2-4.6 mL

of the UV filter working solution (depending on the IL). Next, an aqueous solution containing a specific mass of halide-based IL was added to the solution (see Table B2). To ensure a fair comparison, the amount of each IL was calculated to yield approximately 25  $\mu\text{L}$  of the  $[\text{NTf}_2^-]$ -based IL after the metathesis reaction. Table B2 shows the amount of each IL added to the aqueous analyte solution in order to produce 25  $\mu\text{L}$  of extraction phase. The IL was completely dissolved into the sample solution by vigorous shaking for 10 s. An aqueous solution of  $\text{LiNTf}_2$  ( $0.4 \text{ g mL}^{-1}$ ) was then added to achieve a 1:1 molar ratio of IL to  $\text{LiNTf}_2$ . The tube was then vortexed for 10 s and centrifuged for 5 min at 4500 rpm. A 20  $\mu\text{L}$  aliquot of the hydrophobic IL solvent was then withdrawn *via* micropipette and transferred to a 10 mL headspace vial for HS-GC analysis.

To observe the effect of headspace volume on extraction efficiency, 9.4 mL of ultrapure water containing 200  $\mu\text{g L}^{-1}$  of ES, BS, HS, BP3, MA, EMC and 1  $\text{mg L}^{-1}$  of ETO, EPP was added to a 14 mL round bottom centrifuge tube. Next, an aqueous solution containing 80 mg of  $[\text{BMIM}^+][\text{Br}^-]$  IL was added to the solution. The IL was completely dissolved into the sample solution by vigorous shaking for 10 s. An aqueous solution of  $\text{LiNTf}_2$  ( $0.4 \text{ g mL}^{-1}$ ) was then added to achieve a 1:1 molar ratio of IL to  $\text{LiNTf}_2$ . The sample solution immediately became cloudy due to the metathesis reaction and the formation of the hydrophobic  $[\text{BMIM}^+][\text{NTf}_2^-]$  IL. The tube was then vortexed for 30 s and centrifuged for 5 min at 4500 rpm. Approximately 25  $\mu\text{L}$  of the hydrophobic IL containing preconcentrated UV filters was formed at the bottom of the centrifuge tube. A 20  $\mu\text{L}$  aliquot of  $[\text{BMIM}^+][\text{NTf}_2^-]$  IL was then withdrawn *via* micropipette and transferred to a 10 mL headspace vial containing 12.5 g of glass beads (3 mm diameter) and a smaller flat bottom 2 mL Agilent Technologies HPLC

autosampler vial with the neck removed for HS-GC-MS analysis at 200 °C [27]. A graphical representation of the procedure is shown in Fig. B6.

### 3.3 Results and Discussion

#### 3.3.1 Optimization of the HS-GC-MS step

The aim of this study is to exploit the tunability of ILs to provide a means of preconcentrating analytes into the IL phase during the *in situ* DLLME process while also taking advantage of their non-volatility in direct HS-GC-MS analysis. The HS sampler unit in the HS-GC-MS system operates heating and pressurization of the headspace vial allowing for volatilization of the vial components. The volatile components are then directly transferred to the GC inlet, followed by separation and detection by GC-MS. Thereby, the key point of the HS-GC-MS is the optimization of the HS step. In this particular application, the optimized parameters were the HS oven temperature and the HS sampling volume. The remaining conditions of the HS-GC-MS system are detailed in Section 2.3.

#### 3.3.2 Effect of the headspace temperature

Temperature plays a pivotal role in the response of analytes in HS sampling. In theory, increasing the temperature can increase the amount of analyte that partitions into the headspace, but can also lead to an increase in chromatographic background if volatilization of the solvent occurs [27]. The effect of the HS oven temperature on the response of 8 UV filters was examined by incubating 20  $\mu\text{L}$  of the  $[\text{BMIM}^+][\text{NTf}_2^-]$  IL after *in situ* DLLME at different headspace oven temperatures for 10 min. Fig. 3.1(A) shows that the response of analytes was greatly enhanced as the HS oven temperature was increased from 150 °C to 200 °C. Due to the

semi-volatility of the analytes, increased temperature was observed to influence their desorption into the HS resulting in an increased analyte response.

It is important to point out that no significant chromatographic background was observed in the temperature range studied. Temperatures higher than 200 °C revealed the presence of background peaks due to the partial degradation/volatilization of the IL that overlapped with analyte peaks. Thus, to avoid interference with analyte peaks, a headspace oven temperature of 200 °C was used for all remaining experiments. The HS sampling volume is another important factor in HS-GC-MS. Previous studies reported that decreasing the volume of the HS system may result in an increased response of analytes [27]. The smallest commercially-available HS sampling vial has a capacity of 10 mL. To produce a smaller headspace using vials that are compatible with the headspace system, a modified HS sampling vial was developed following the procedure described by Zhang *et al.* [27].

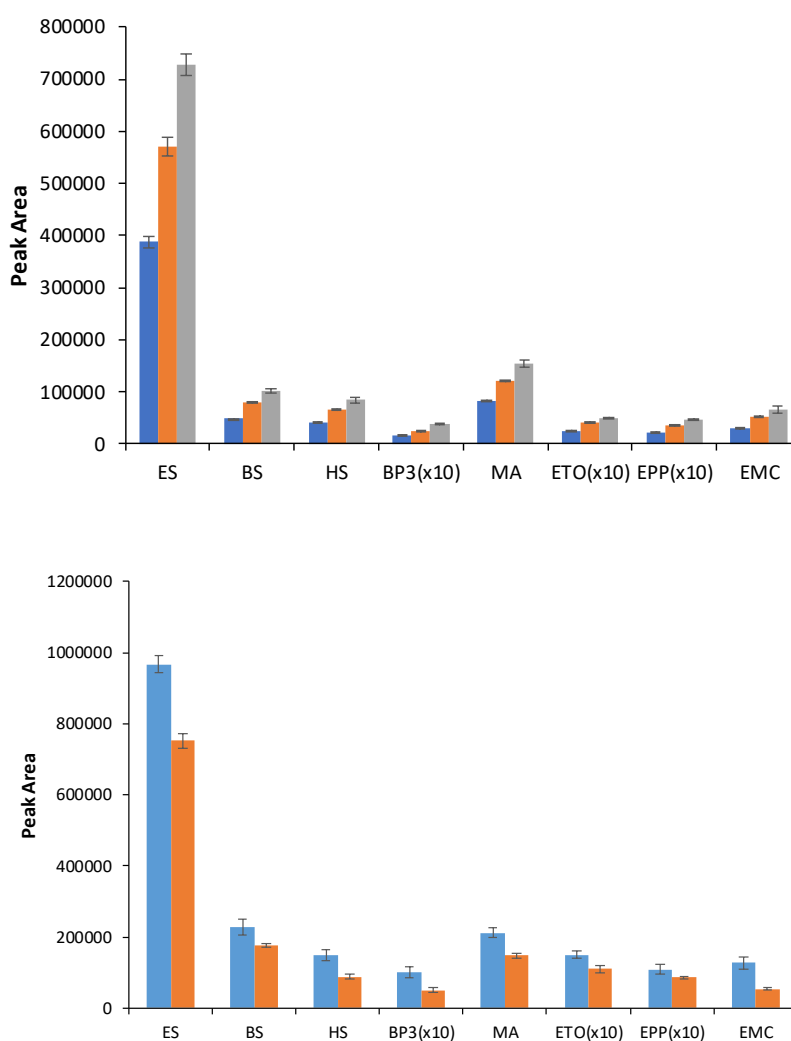
### 3.3.3 Influence of the headspace sampling volume

Briefly, 10 mL HS sampling vials were filled with glass beads, and a glass insert with a flat bottom was placed inside the vial resulting in a reduced volume of 4.2 mL (see Fig. B2). Fig 3.1(B) shows that as the HS volume was decreased from the standard 10 mL HS vial to the adjusted 4.2 mL HS vial, the extraction efficiency of all analytes increased by 15-40%. Due to the increased response of analytes, a 4.2 mL HS volume was selected as optimum in this study.

### 3.3.4 Design of ionic liquids for in situ IL-DLLME

UV filters are known to contain many functional groups including aromatic, alcohol, ketone, ester, amine, and aliphatic moieties that may influence their partitioning behavior from the aqueous solution into the extraction phase. Five different imidazolium-based ILs, shown in Table 3.1, were designed to examine various intermolecular interactions with the analytes

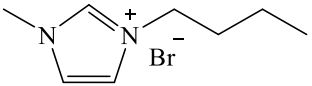
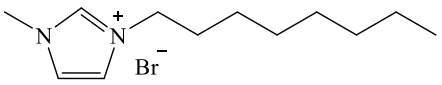
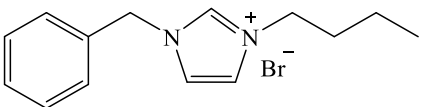
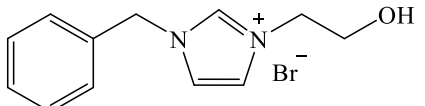
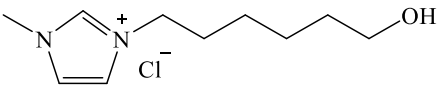
and their effect on extraction efficiency. The  $[\text{BMIM}^+][\text{Br}^-]$  IL has been utilized as an extraction solvent in other *in situ* DLLME studies [24, 27] and was used as a reference IL.



**Figure 3.1.** (A) Effect of headspace incubation temperature on extraction efficiencies (expressed in peak area) of UV filters from 5 mL of ultrapure water at (■) 150 °C, (■) 180 °C, and (■) 200 °C, and (B) Effect of headspace volume on the extraction efficiency (expressed in peak area) of UV filters from 5 mL of ultrapure water. (■) 4.2 mL modified headspace vial, (■) 10 mL headspace vial.  $[\text{BMIM}^+][\text{Br}^-]$  volume: 20  $\mu\text{L}$ ; headspace incubation temperature: 200 °C; IL:NTf<sub>2</sub> = 1:1; Concentration of analytes ETO and EPP: 1 mg L<sup>-1</sup>; Concentration of the remaining analytes: 200  $\mu\text{g L}^{-1}$ ; Vortex time: 10 s.

To examine hydrophobic interactions between the IL solvent and the UV filters, an octyl moiety was incorporated as a substituent on the imidazolium cation structure to produce the [OMIM<sup>+</sup>][Br<sup>-</sup>] IL. To investigate hydrogen bonding interactions between the IL and UV filters, the butyl chain of [BMIM<sup>+</sup>][Br<sup>-</sup>] was replaced with a hexanol moiety to produce the [HeOHMIM<sup>+</sup>][Cl<sup>-</sup>] IL. The methyl group substituent within the [BMIM<sup>+</sup>][Br<sup>-</sup>] IL was replaced with a benzyl moiety ([BeBIM<sup>+</sup>][Br<sup>-</sup>]) to examine the importance of  $\pi$ - $\pi$  interactions on extraction efficiency. Lastly, an IL containing both benzyl and hydroxyl groups was synthesized ([BeEOHIM<sup>+</sup>][Br<sup>-</sup>]) to examine the effect of combined interactions on the extraction efficiency of UV filters from an aqueous sample.

**Table 3.1.** Chemical structures of ILs as well as the volumes of IL and LiNTf<sub>2</sub> solution applied for *in situ* DLLME analysis of UV filters from 10 mL of aqueous solution. The employed volumes were used to produce approximately 25  $\mu$ L of [NTf<sub>2</sub><sup>-</sup>]-based IL.

Structure	Abbreviation	Volume of the IL solution added ( $\mu$ L) <sup>a</sup>	Volume of the LiNTf <sub>2</sub> solution added ( $\mu$ L) <sup>b</sup>
	[BMIM <sup>+</sup> ][Br <sup>-</sup> ]	400	265 <sup>c</sup> 400 <sup>d</sup>
	[OMIM <sup>+</sup> ][Br <sup>-</sup> ]	180	95 <sup>c</sup> 145 <sup>d</sup>
	[BeBIM <sup>+</sup> ][Br <sup>-</sup> ]	200	100 <sup>c</sup> 150 <sup>d</sup>
	[BeEOHIM <sup>+</sup> ][Br <sup>-</sup> ]	560	285 <sup>c</sup> 430 <sup>d</sup>
	[HeOHMIM <sup>+</sup> ][Cl <sup>-</sup> ]	770	505 <sup>c</sup> 760 <sup>d</sup>

<sup>a</sup> The IL solution was prepared by dissolving 2 g of IL in 10 mL of ultrapure water.

<sup>b</sup> The LiNTf<sub>2</sub> solution was prepared by dissolving 4 g of LiNTf<sub>2</sub> in 10 mL of ultrapure water.

<sup>c</sup> Molar ratio of IL:LiNTf<sub>2</sub>=1:1.

<sup>d</sup> Molar ratio of IL:LiNTf<sub>2</sub>=1:1.5.

The extraction efficiencies obtained in ultrapure water were compared for the five designed ILs. Given the different solubility of the  $[\text{NTf}_2^-]$  form of the ILs in the aqueous sample, adding equal mass of each halide-based IL resulted in different amounts of sedimented phase after *in situ* DLLME. To ensure a fair comparison of each IL, the amount of each IL used was estimated to yield approximately 25  $\mu\text{L}$  of the  $[\text{NTf}_2^-]$ -based IL after DLLME, as shown in Table 3.1. To avoid the aqueous solution being transferred to the HS vial, only 20  $\mu\text{L}$  of the sedimented IL phase was pipetted for HS-GC-MS analysis. Fig. 3.2 shows a comparison of extraction efficiency for all ILs used in this study. The  $[\text{BMIM}^+][\text{Br}^-]$  and  $[\text{BeEOHIM}^+][\text{Br}^-]$  ILs exhibited the highest extraction efficiencies for most of the UV filters. It can be noted that ETO and EPP were not significantly extracted using any of the ILs as extraction solvents, even at relatively high concentrations (milligram per liter level). If the chemical structures of EPP and ES are compared, EPP is an aminobenzoate and ES a salicylate derivative. Thus, the main difference between these two compounds is that EPP possesses a tertiary amine in its chemical structure while ES has a hydroxyl functional group. However, only ES is extracted at low concentration levels using *in situ* DLLME, which indicates that the designed ILs appear to be more beneficial in the extraction of analytes possessing hydroxyl functional groups.

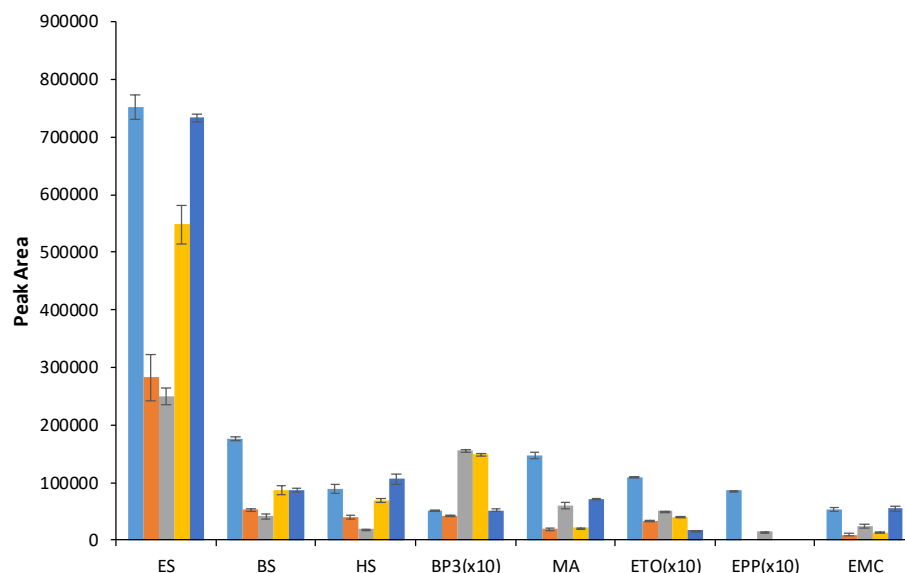


**Figure 3.2.** Extraction comparison for UV filters extracted from 5 mL of ultrapure water using 20  $\mu\text{L}$  of (■) [BMIM<sup>+</sup>][Br<sup>-</sup>], (■) [OMIM<sup>+</sup>][Br<sup>-</sup>], (■) [BeBIM<sup>+</sup>][Br<sup>-</sup>], (■) [HeOHMIM<sup>+</sup>][Cl<sup>-</sup>], (■) [BeEOHIM<sup>+</sup>][Br<sup>-</sup>] ILs. Headspace incubation temperature: 200 °C; IL:NTf<sub>2</sub> = 1:1; Concentration of analytes ETO and EPP: 1 mg L<sup>-1</sup>; Concentration of the remaining analytes: 200  $\mu\text{g L}^{-1}$ ; Vortex time: 10 s

### 3.3.5 Optimization of in situ DLLME

After testing the suitability of different ILs for the extraction of this group of UV filters, the main parameters that influence the *in situ* DLLME procedure were optimized using a factor-by-factor approach. With both [BMIM<sup>+</sup>][NTf<sub>2</sub><sup>-</sup>] and [BeEOHIM<sup>+</sup>][NTf<sub>2</sub><sup>-</sup>] exhibiting high extraction efficiency for most of the UV filters, the [BMIM<sup>+</sup>][Br<sup>-</sup>] IL was chosen for optimization for two reasons: (1) less IL mass was needed for extraction, and (2) [BMIM<sup>+</sup>][Br<sup>-</sup>] requires less work up during synthesis. The optimized parameters included the amount of sedimented IL phase after extraction, total extraction volume, IL to ion-exchange reagent ratio, ionic strength, pH, and vortex time. The criteria for the optimization was to achieve the highest extraction efficiencies for the UV filters. Thereby, conditions that resulted in the highest peak areas were used for subsequent extractions.



### 3.3.6 Effect of the amount of sedimented phase after extraction,

The amount of sedimented phase after *in situ* DLLME influences the extraction as it is directly related to the preconcentration of the method. The amount of the sedimented phase is proportional to the initial volume of halide-based IL used in the extraction. Thus, this volume was varied to generate volumes of sedimented [BMIM<sup>+</sup>][NTf<sub>2</sub><sup>-</sup>] IL ranging from 15-60 μL. Fig. 3.3 shows that similar extraction efficiencies of UV filters were obtained when 15-25 μL of hydrophobic IL was used. However, further increasing the IL volume to 40 μL and 60 μL resulted in lower extraction efficiencies of the target analytes. Decreases in extraction efficiencies with large amounts of IL as extraction solvent have also been reported in previous studies [27]. Thus, the amount of halide-based IL to obtain a sedimented IL volume of 25 μL was used for subsequent extractions.

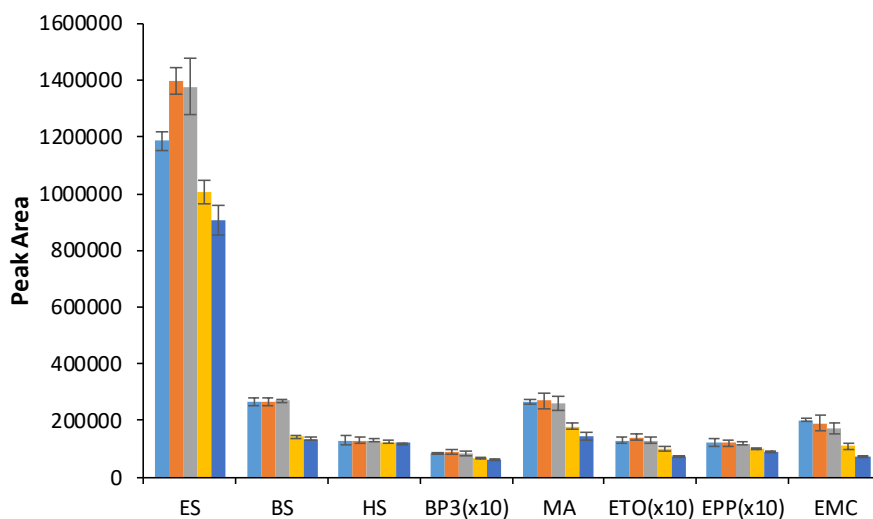


**Figure 3.3.** Effect of the amount of sedimented IL phase after extraction (expressed in peak area) of UV filters from 10 mL of ultrapure water. [BMIM<sup>+</sup>][Br<sup>-</sup>] volume: (■) 15 μL, (■) 20 μL, (■) 25 μL, (■) 40 μL, (■) 60 μL. Headspace incubation temperature: 200 °C; IL:NTf<sub>2</sub> = 1:1; Concentration of analytes ETO and EPP: 1 mg L<sup>-1</sup>; Concentration of the remaining analytes: 200 μg L<sup>-1</sup>; Vortex time: 10 s.

### 3.3.7 Influence of the initial sample volume

Total extraction volume can play a significant role in the total amount of analyte in the extraction solution. However, for *in situ* DLLME, increasing the total volume can influence the amount of sedimented IL phase that can be collected at the end of the procedure, which can also impact extraction efficiency. For a fair comparison, the amount of IL added to each of the extractions yielded approximately 25  $\mu\text{L}$  of hydrophobic IL. Aqueous solution volumes of 2.5 mL, 5 mL, and 10 mL were examined to determine their effect on extraction efficiencies. Fig. B7 shows that the volume of the extraction significantly influences extraction efficiency for all analytes in the solution. Increasing the aqueous solution volume lead to a higher extraction efficiency as the maximum preconcentration factor increased from 100 (2.5 mL / 0.025 mL) to 400 (10 mL / 0.025 mL). However, it is important to mention that a higher mass of IL is needed to produce the desired 25  $\mu\text{L}$  of sedimented IL at these conditions because of the partial solubility of the IL in water. Due to the greatly enhanced extraction efficiencies at higher volumes, total sample volumes of 10 mL were used for further experiments.

### 3.3.8 Effect of the IL to metathesis reagent ratio

Two different molar ratios of IL to  $\text{LiNTf}_2$  (1:1 and 1:1.5) were studied to examine the effect of the ion exchange reagent on the extraction efficiency of UV filters. As shown in Fig. 3.4, increasing the molar ratio from 1:1 to 1:1.5 led to a significant decrease in extraction efficiency for all analytes. This result is in agreement with other reported *in situ* DLLME studies [24, 27]. It was noted for extractions using molar ratios of 1:1.5 that the sedimented IL phase was distinctly cloudy in comparison to the sedimented IL phase formed from the 1:1 molar ratio. Due to the ionic nature of both the metathesis reagent and the IL, a possible explanation of this phenomenon is that the excess metathesis reagent may saturate the IL

resulting in less preconcentration of the analyte. A 1:1 (IL to LiNTf<sub>2</sub>) molar ratio was used for subsequent extractions.

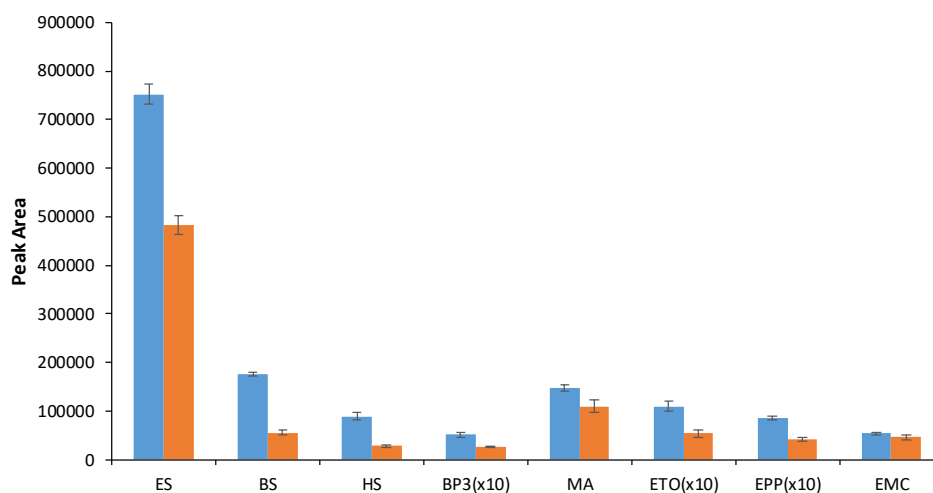


**Figure 3.4.** Effect of molar ratio of the [BMIM<sup>+</sup>][Br<sup>-</sup>] IL and LiNTf<sub>2</sub> on the extraction efficiency (expressed in peak area) of UV filters from 5 total sample volume. (■) IL:NTf<sub>2</sub> = 1:1, (■) IL:NTf<sub>2</sub> = 1:5. [BMIM<sup>+</sup>][Br<sup>-</sup>] volume: 20 μL; headspace incubation temperature: 200 °C; Concentration of analytes ETO and EPP: 1 mg L<sup>-1</sup>; Concentration of the remaining analytes: 200 μg L<sup>-1</sup>; Vortex time: 10 s.

### 3.3.9 Influence of ionic strength and pH

The addition of a kosmotropic salt is performed in many microextraction procedures to decrease the solubility of the analytes in the aqueous phase and thus increase their partitioning into the organic phase, thereby improving extraction efficiency of the analyte. To determine the effect of salt on the analyte extraction efficiency, NaCl was added to the aqueous solution at 3.5% and 5% (w/v). Fig. B8 shows that as the concentration of NaCl is increased, the extraction efficiency is slightly reduced for all of the analytes. With an increase in salt concentration, it was observed that the sedimented IL phase after DLLME appeared slightly cloudy.

Previous DLLME methods reported mildly acidic pH having a slightly enhanced effect on extraction efficiency of UV filters containing phenolic moieties [28]. In order to examine the effect of pH on the extraction efficiencies of target analytes using the developed *in situ* DLLME method, extractions were performed at pH 4, 6, 8, and 10. The aqueous solution pH was adjusted to the appropriate value using HCl or NaOH. Fig. B9 shows that no significant changes in extraction efficiencies were observed for all analytes over the range of pH conditions tested, with the analyte ES showing a slight increase in its extraction efficiency at pH 4. Given these results, all subsequent extractions were performed without any pH adjustment.

#### 3.3.10 Influence of vortex time

Agitation of the extraction solution via vortex has been shown to have a substantial impact on extraction efficiency in DLLME methods [28]. In order to ensure proper mixing of analytes and the hydrophobic IL phase, vortex times of 10 s, 30 s, and 60 s were examined. An increase in extraction for all analytes was observed as the vortex time was increased from 10 s to 30 s, as shown in Fig. 3.5. Further increasing the vortex time to 60 s resulted in no significant increase in extraction efficiencies. In addition, a vortex time of 60 s resulted in poorer reproducibility compared to those at 10 s and 30 s. Therefore, vortex time of 30 s was used for all subsequent experiments.

#### 3.3.11 Analytical performance

The analytical performance of the two best performing ILs, namely, [BMIM<sup>+</sup>][Br<sup>-</sup>] and [BeEOHIM<sup>+</sup>][Br<sup>-</sup>], was evaluated for the extraction of the target UV filters. Tables 3.2 and 3.3 show the figures of merit based on five- to seven-point calibration curves for [BMIM<sup>+</sup>][Br<sup>-</sup>] and [BeEOHIM<sup>+</sup>][Br<sup>-</sup>], respectively.

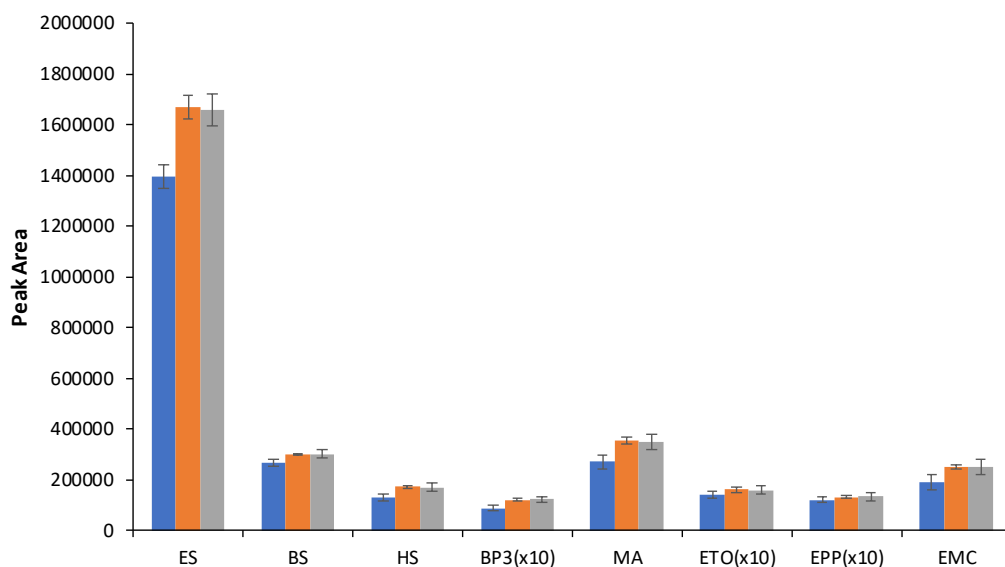


**Figure 3.5.** Effect of vortex time on extraction efficiencies (expressed in peak area) of UV filters from 10 mL of ultrapure water. (■) 10 s vortex, (■) 30 s vortex, and (■) 60 s vortex. [BMIM<sup>+</sup>][Br<sup>-</sup>] volume: 20  $\mu$ L; IL:NTf<sub>2</sub> = 1:1; Headspace incubation temperature: 200 °C; Concentration of analytes ETO and EPP: 1 mg L<sup>-1</sup>; Concentration of the remaining analytes: 200  $\mu$ g L<sup>-1</sup>

Similar linear ranges were obtained for the two ILs with most of the analytes exhibiting linear ranges from 50 to 500  $\mu$ g L<sup>-1</sup>. The analytes ETO and EPP were omitted due to poor extraction below the milligram per liter concentration level. All analytes showed good linearity with coefficient of determination ( $R^2$ ) values ranging from 0.997 to 0.999.

**Table 3.2.** Figures of merit for IL *in situ* DLLME analysis of UV filters in ultrapure water using the [BMIM<sup>+</sup>][Br<sup>-</sup>] IL.

Analyte	Linear Range ( $\mu$ g L <sup>-1</sup> )	Slope $\pm$ error	LOD ( $\mu$ g L <sup>-1</sup> )	$R^2$	%RR <sup>a</sup>	
					Pool Water	Lake Water
ES	50-500	4392 $\pm$ 203	0.50	0.998	106	108
BS	50-500	1932 $\pm$ 64	1.0	0.998	101	103
HS	50-500	1602 $\pm$ 14	1.0	0.999	117	115
BP3	25-500	273 $\pm$ 25	10	0.997	109	101
MA	50-500	2324 $\pm$ 58	1.0	0.998	101	99.7
EMC	50-500	784 $\pm$ 31	1.0	0.998	104	106

<sup>a</sup> % relative recovery calculated at analyte concentration of 50  $\mu$ g L<sup>-1</sup>.

**Table 3.3.** Figures of merit for IL *in situ* DLLME analysis of UV filters in ultrapure water using the [BeEOHIM<sup>+</sup>][Br<sup>-</sup>] IL.

Analyte	Linear Range ( $\mu\text{g L}^{-1}$ )	Slope $\pm$ error	LOD ( $\mu\text{g L}^{-1}$ )	R <sup>2</sup>	%RR <sup>a</sup>	
					Pool Water	Lake Water
ES	50-500	4059 $\pm$ 198	0.50	0.998	109	110
BS	50-500	1258 $\pm$ 52	1.0	0.998	102	104
HS	50-500	1630 $\pm$ 13	0.50	0.999	117	119
BP3	25-500	319 $\pm$ 10	5.0	0.997	102	108
MA	50-250	1311 $\pm$ 42	1.0	0.998	101	98.1
EMC	50-500	728 $\pm$ 55	1.0	0.998	99.8	107

<sup>a</sup> % relative recovery calculated at analyte concentration of 50  $\mu\text{g L}^{-1}$ .

The limit of detection (LOD) for each analyte was determined by decreasing the spiked analyte concentration until a signal to noise (S/N) ratio of 3:1 was attained. The LODs for UV filters using the [BMIM<sup>+</sup>][Br<sup>-</sup>] and [BeEOHIM<sup>+</sup>][Br<sup>-</sup>] ILs ranged from 0.5 to 10  $\mu\text{g L}^{-1}$  and 0.5 to 5  $\mu\text{g L}^{-1}$ , respectively. The precision of the method was evaluated by the estimating the percent relative standard deviation (%RSD) obtained after intra-day experiments at a spiked level of 50  $\mu\text{g L}^{-1}$ . The RSD values ranged between 3.9% and 13.6%.

### 3.3.12 Analysis of real samples

In order to further examine the performance of the developed IL *in-situ* DLLME method, extractions were performed from two real water samples, including pool water and lake water. Pool water was collected and used without further treatment. Lake water was subjected to filtration with a 0.45  $\mu\text{m}$  filter to remove any particulates from the sample. For the [BMIM<sup>+</sup>][Br<sup>-</sup>] IL, no analytes were detected in any of the studied samples. Similarly, the [BeEOHIM<sup>+</sup>][Br<sup>-</sup>] IL showed no observable peaks in the non-spiked real samples. Tables 3.2 and 3.3 show the relative recovery (RR) values of the 6 UV filters after extraction with the [BMIM<sup>+</sup>][Br<sup>-</sup>] and the [BeEOHIM<sup>+</sup>][Br<sup>-</sup>] ILs, respectively. All RR values were obtained at the 50  $\mu\text{g L}^{-1}$  level from pool and lake water samples. For the [BMIM<sup>+</sup>][Br<sup>-</sup>] IL, RR values of UV

filters in pool water ranged from 101% to 117%, while they ranged from 99.7% to 115% when lake water was used as a sample matrix. The [BeEOHIM<sup>+</sup>][Br<sup>-</sup>] IL resulted in RR values ranging from 99.8% to 117% in pool water and from 98.1% to 119% for lake water. The RSD obtained for these experiments was lower than 14.2% in all cases. These results suggest that the matrix effects were relatively similar for pool and lake water when both ILs were used as extraction solvents. The obtained relative recovery values demonstrate the robustness of the developed *in-situ* DLLME method for the extraction of UV filters using ionic liquids.

A comparison of the developed method to other microextraction techniques that have been reported for the determination of UV filters is shown in Table B3. In comparison with other DLLME methods, this approach exploits the use of (ILs) for *in situ* DLLME. To the best of our knowledge, this is the first time that this *in situ* DLLME procedure has been applied towards the extraction of UV filters. Furthermore, this method provides an alternative to other techniques such as SPME, which generally require long sampling times. Compared to both SPME and SBS $\mu$ E methods, the proposed *in situ* DLLME method is between ~3–7 times faster. Furthermore, this method allows for many samples to be prepared at the same time (as many as the centrifuge allows), permitting rapid high throughput screening of UV filters in real samples while achieving similar sensitivity. In this particular application, 6 extractions were simultaneously performed, in ~7–10 min. In comparison, reported SPME procedures requires 25–75 min of extraction time per sample [2, 16].

### 3.4 Conclusions

In this study, a *in situ* DLLME method coupled to HS-GC-MS was developed for the determination of UV filters using ILs as extraction solvents. Five ILs with different chemical

structures were employed and their selectivities toward the target UV filters were assessed. The highest extraction efficiencies of the target analytes were obtained using the [BMIM<sup>+</sup>][Br<sup>-</sup>] and [BeEOHIM<sup>+</sup>][Br<sup>-</sup>] ILs. After proper optimization, the developed methods with both ILs exhibited adequate precision and linearity, and LODs of six UV filters at the low microgram per liter level in aqueous samples. The method was successfully applied for the analysis of pool and lake water samples with no significant observable matrix effect. Overall, the developed *in situ* IL-based DLLME coupled with HS-GC-MS resulted in a rapid sample preparation technique for high throughput analysis, constituting an advantage over other methods such as SPME and SBS DME which require much longer extraction times. Continued studies focusing on further tuning of the IL structure for a highly selective determination of target analytes from complex environmental or biological samples are currently underway.

### Acknowledgements

The authors acknowledge funding from the Chemical Measurement and Imaging Program at the National Science Foundation (Grant number CHE-1709372).

### References

- [1] L. Vidal, A. Chisvert, A. Canals, A. Salvador, *Talanta* 81 (2010) 549
- [2] M. Vila, M. Celeiro, J.P Lamas, T. Dagnac, *Anal. Methods* 8 (2016) 7069
- [3] J.L Benedé, A. Chisvert, A. Salvador, D. Sánchez-Quiles, A. Tovar-Sánchez, *Anal. Chim. Acta* 812 (2014) 50
- [4] M. Vila, M. Celeiro, J.P. Lamas, C. Garcia-Jares, T. Dagnac, M. Llompart, *Hazard Mater.* 323 (2017) 45



- [5] F. Vela-Soria, M.E. Gallardo-Torres, O. Ballesteros, C. Diaz, J. Perez, A. Navalon, M.F. Fernandez, N.J. Olea, *Chromatogr. A* 1487 (2017) 153
- [6] D.L. Giokas, A. Salvador, A. Chisvert, *Trends Anal. Chem.* 26 (2007) 360
- [7] M. Vila, J.P. Lamas, C. Garcia-Jares, T. Dagnac, M. Llompart, *Chromatogr. A* 1405 (2015) 12
- [8] J.L. Benede, A. Chisvert, D.L. Giokas, A. Salvador, *Talanta* 147 (2016) 246
- [9] I.P. Roman, A. Chisvert, A. Canals, *J. Chromatogr. A* 1218 (2011) 2467
- [10] H. Zhang, H.K. Lee, *Anal. Chim. Acta* 742 (2012) 67
- [11] S.C. Cunha, A. Pena, J.O. Fernandes, *J. Chromatogr. A* 1414 (2015) 10
- [12] M. Vila, J.P. Lamas, C. Garcia-Jares, T. Dagnac, M. Llompart, *Microchem. J.* 124 (2016) 530
- [13] K.T. Nguyen, C. Scapolla, M. Di Carro, E. Magi, *Talanta* 85 (2011) 2375
- [14] M. Meinerling, M. Daniels, *Anal. Bioanal. Chem.* 386 (2006) 1465
- [15] S. Armenta, S. Garrigues, M. de la Guardia, *Trends Anal. Chem.* 27 (2008) 497
- [16] J. An, J.L. Anderson, *Talanta* 182 (2018) 74
- [17] M.J. Trujillo-Rodriguez, H. Nan, J.L. Anderson, *J. Chromatogr. A* 1540 (2018) 11
- [18] N. Negreira, I. Rodriguez, M. Ramil, E. Rubi, R. Cela, *Anal. Chim. Acta* 638 (2009) 36
- [19] I. Tarazona, A. Chisvert, Z. Leon, A. Salvador, *J. Chromatogr. A* 1217 (2010) 4771
- [20] L. Vidal, A. Chisvert, A. Canals, A. Salvador, *J. Chromatogr. A* 1174 (2007) 95
- [21] D. Ge, H.K. Lee, *J. Chromatogr. A* 1229 (2012) 1
- [22] J. An, M.J. Trujillo-Rodriguez, V Pino, J.L. Anderson, *J. Chromatogr. A* 1500 (2017) 1
- [23] T.D. Ho, C. Zhang, L.W. Hantao, J.L. Anderson, *Anal. Chem.* 86 (2014) 262
- [24] C. Yao, J.L. Anderson, *Anal. Bioanal. Chem.* 395 (2009) 1491

- [25] M. Baghdadi, F. Shemirani, Anal. Chim. Acta 634 (2009) 186
- [26] M.J. Trujillo-Rodríguez, P. Rocío-Bautista, V. Pino, A.M. Afonso, Trends Anal. Chem. 51 (2013) 87
- [27] C. Zhang, C. Cagliero, S.A. Pierson, J.L. Anderson, J. Chromatogr. A 1481 (2017) 1
- [28] I. Tarazona, A. Chisvert, A. Salvador, Anal. Methods 6 (2014) 7772
- [29] B. Kolb, J. Chromatogr. A 842 (1999) 163
- [30] N.H. Snow, Trends Anal. Chem. 21 (2002) 608
- [31] J.C. Flórez Menéndez, M.L. Fernández Sánchez, J.E. Sánchez Uria, E. Fernández Martinez, A. Sanz-Medel, Anal. Chim. Acta 415 (2000) 9
- [32] H. Yu, K.D. Clark, J.L. Anderson, J. Chromatogr. A 1406 (2015) 10

## CHAPTER 4

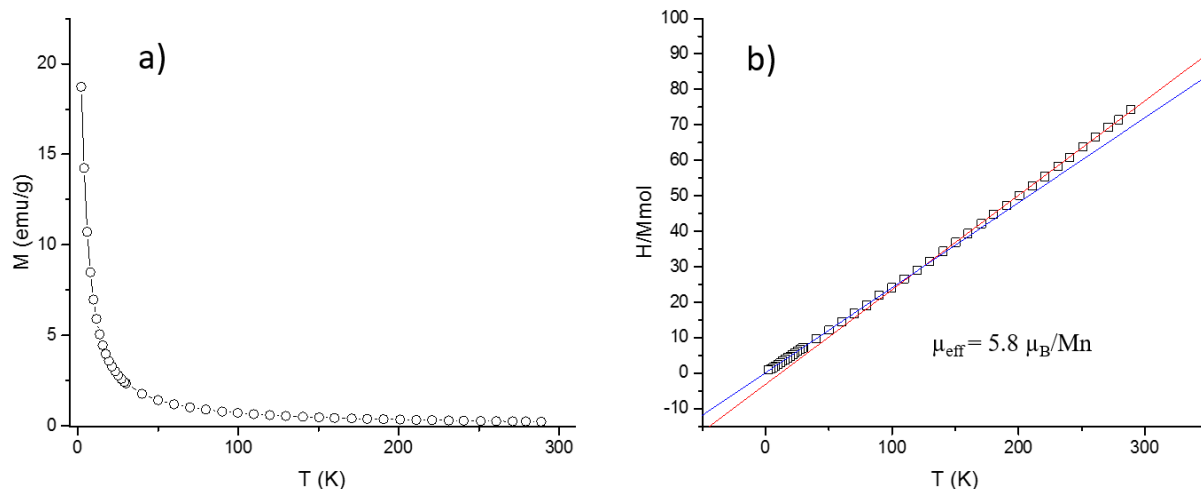
### GENERAL CONCLUSIONS

This thesis summarizes the synthesis of ILs and MILs for their application in microextraction techniques. ILs and MILs developed in these studies were specifically tailored to extend their applications in analytical chemistry as well as overcome the weaknesses of other sample preparation methods.

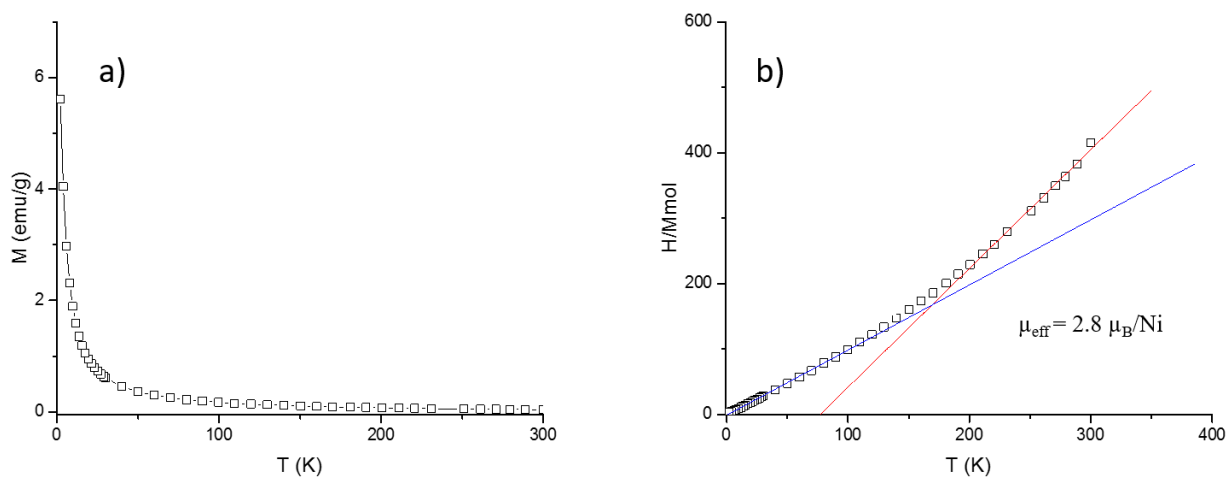
Chapter 2 describes the synthesis of new class of MILs for their application in analytical chemistry. The synthesis of the MILs was achieved in a simple two-step process where both transition and rare earth metals were able to be imparted into the MIL structure. Both the cation and the anion of each MIL possessed features leading to their stability in aqueous environments even at high temperatures. Furthermore, exceptionally low viscosity was achieved in comparison to the existing MILs, giving a plethora of future opportunities for these MILs to be used in many analytical techniques.

Chapter 3 describes the development of an *in situ* DLLME procedure utilizing ILs as extraction solvents coupled to HS-GC-MS. This method demonstrated good extraction capabilities from both pool and lake water samples. Overall, the *in situ* DLLME method takes much less time for the preconcentration of the target analytes compared to other reported methods. Furthermore, this technique allows for many samples to be prepared simultaneously lending itself to high throughput analysis.

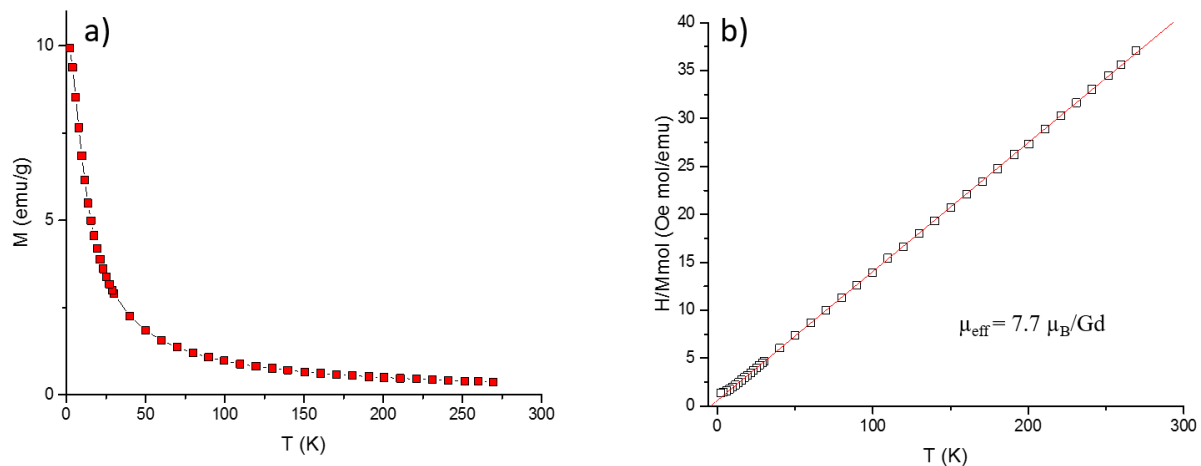
**APPENDIX A**  
**SUPPLEMENTAL INFORMATION ACCOMPANYING**  
**CHAPTER 2**



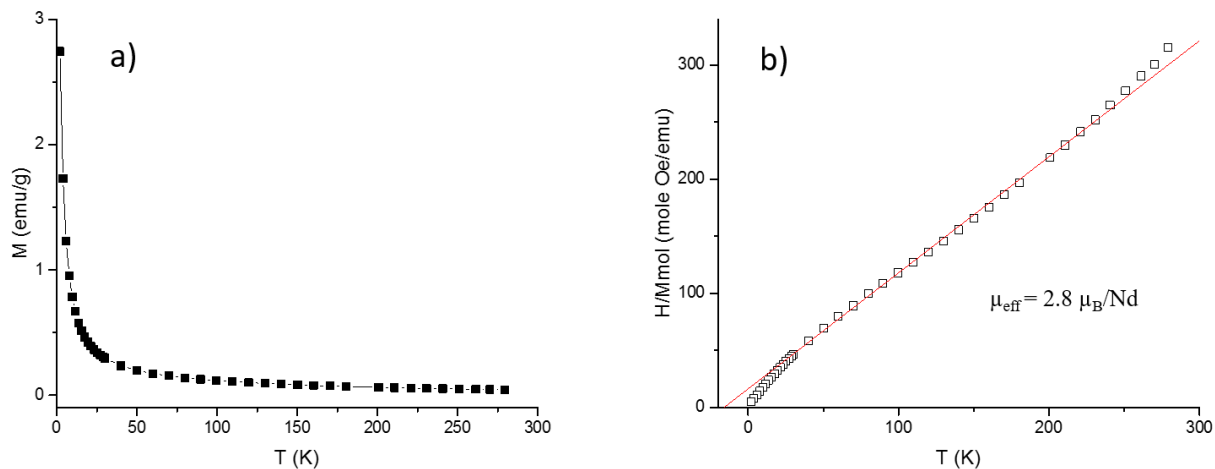
**Figure A1.** (a) Magnetization of the  $[P_{66614}^+][Mn(II)(hfacac)_3^-]$  MIL measured as a function of temperature in a 20000 Oe applied magnetic field (b) Curie-Weiss fits of both high- and low-temperature linear regions of the reciprocal susceptibility



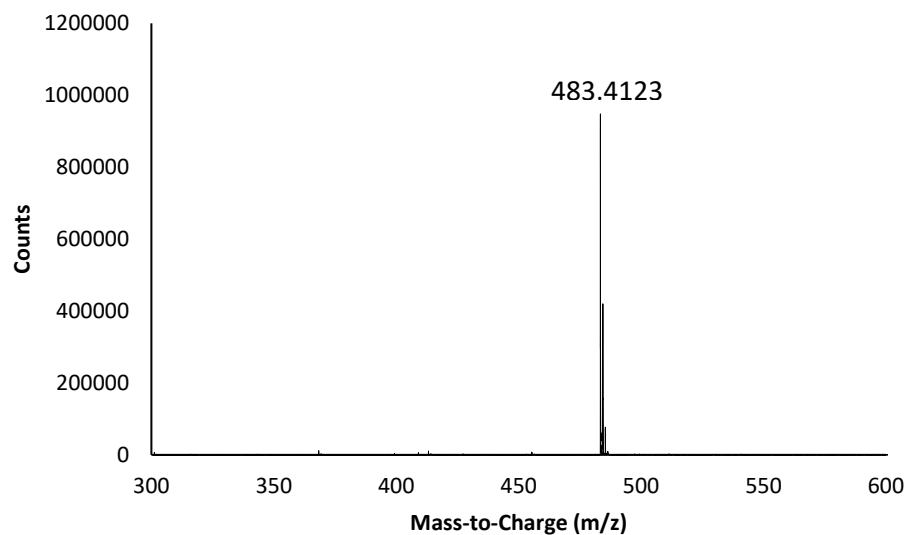
**Figure A2.** (a) Magnetization of the  $[P_{66614}^+][Ni(II)(hfacac)_3^-]$  MIL measured as a function of temperature in a 20000 Oe applied magnetic field (b) Curie-Weiss fits of the linear regions of the reciprocal susceptibility above and below the  $\sim 150$  K anomaly.



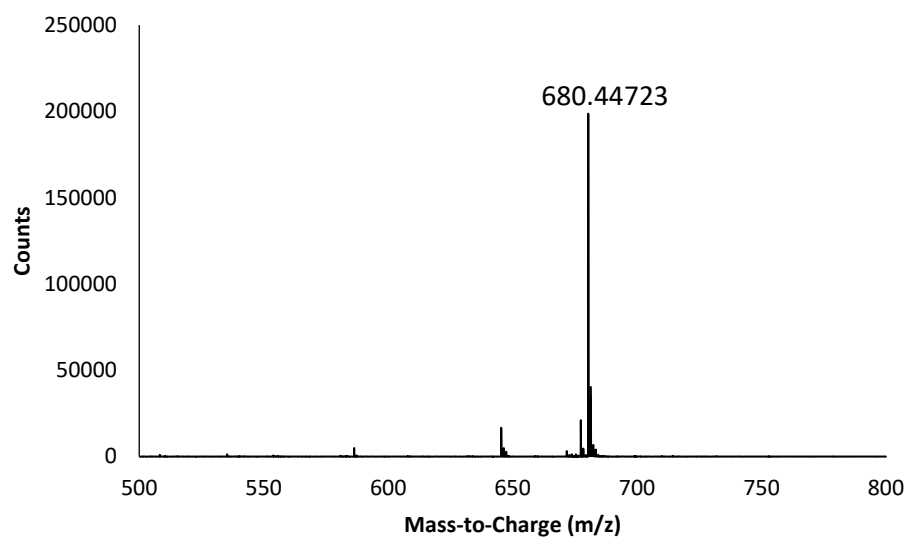
**Figure A3.** (a) Magnetization of the  $[P_{66614}^+][Gd(III)(hfacac)_4^-]$  MIL measured as a function of temperature in a 20000 Oe applied magnetic field (b) Curie-Weiss fit of the linear portion of the reciprocal susceptibility.



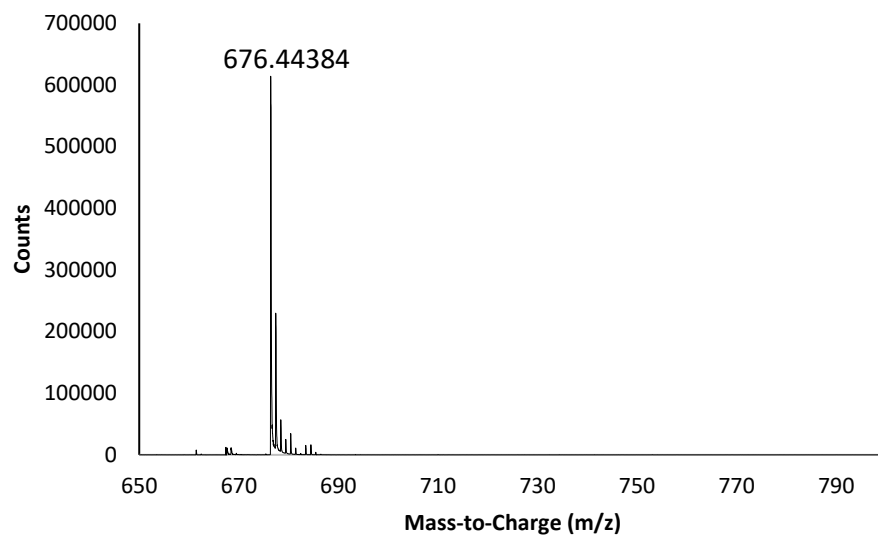
**Figure A4.** (a) Magnetization of the  $[P_{66614}^+][Nd(III)(hfacac)_4^-]$  MIL measured as a function of temperature in a 20000 Oe applied magnetic field (b) Curie-Weiss fit of the linear portion of the reciprocal susceptibility.



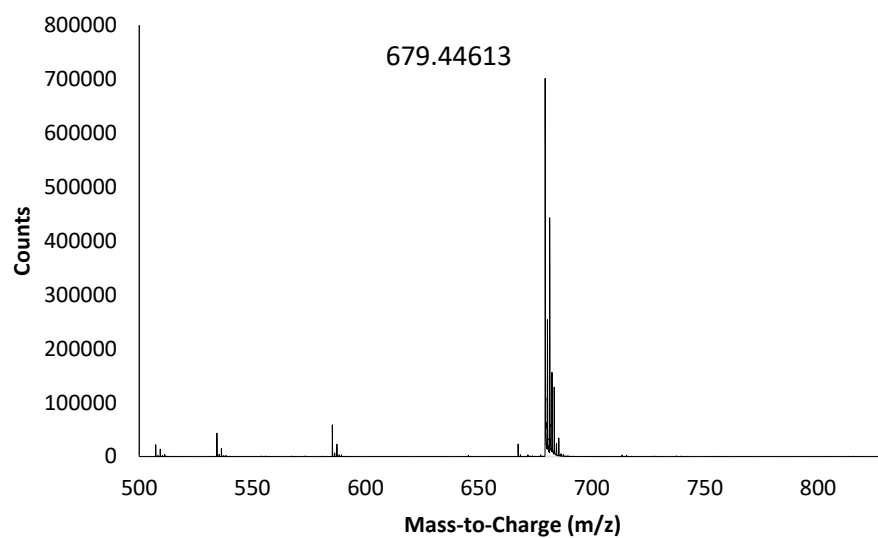
**Figure A5.** Mass spectrum of  $[P_{66614}^+]$  using TOF LC/MS (positive mode).



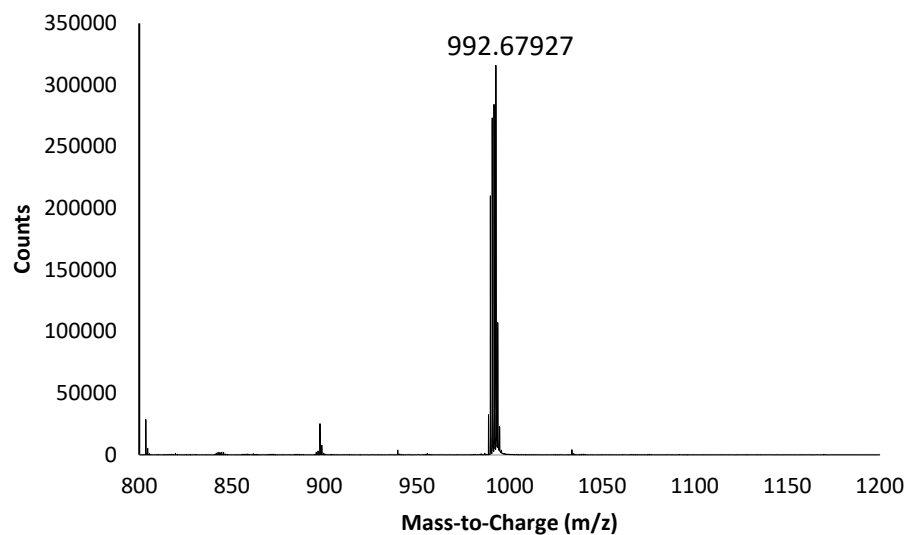
**Figure A6.** Mass spectrum of  $[Co(II)(hfacac)_3^-]$  using TOF LC/MS (negative mode).



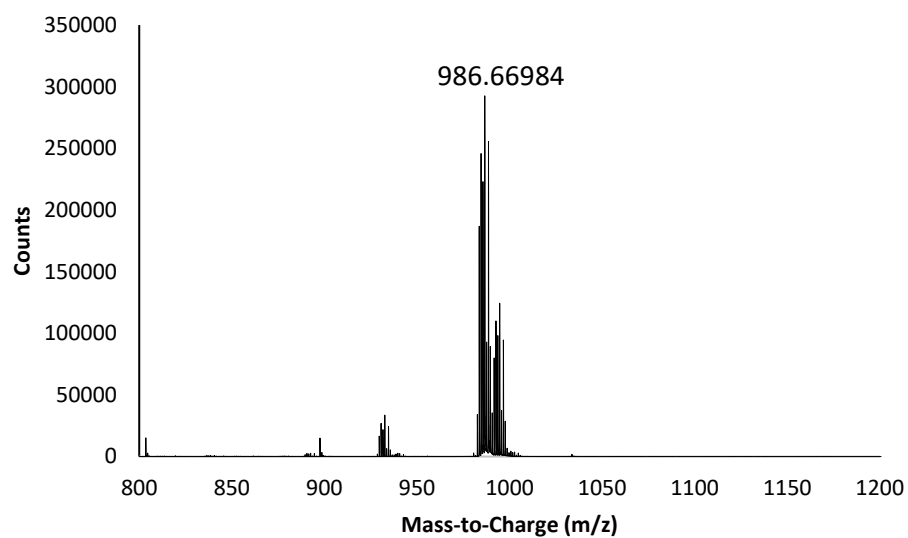
**Figure A7.** Mass spectrum of  $[\text{Mn(II)(hfacac)}_3^-]$  using TOF LC/MS (negative mode).



**Figure A8.** Mass spectrum of  $[\text{Ni(II)(hfacac)}_3^-]$  using TOF LC/MS (negative mode).

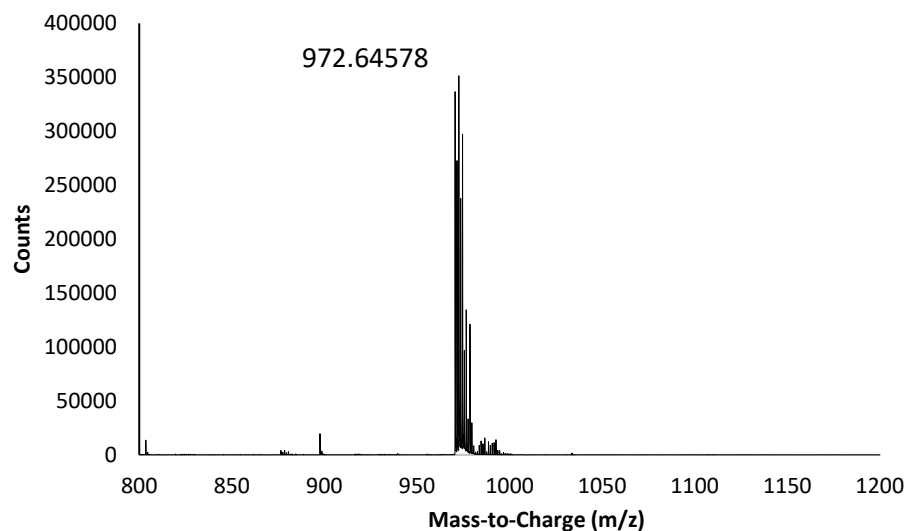


**Figure A9.** Mass spectrum of  $[\text{Dy(III)(hfacac)}_4]^-$  using TOF LC/MS (negative mode).

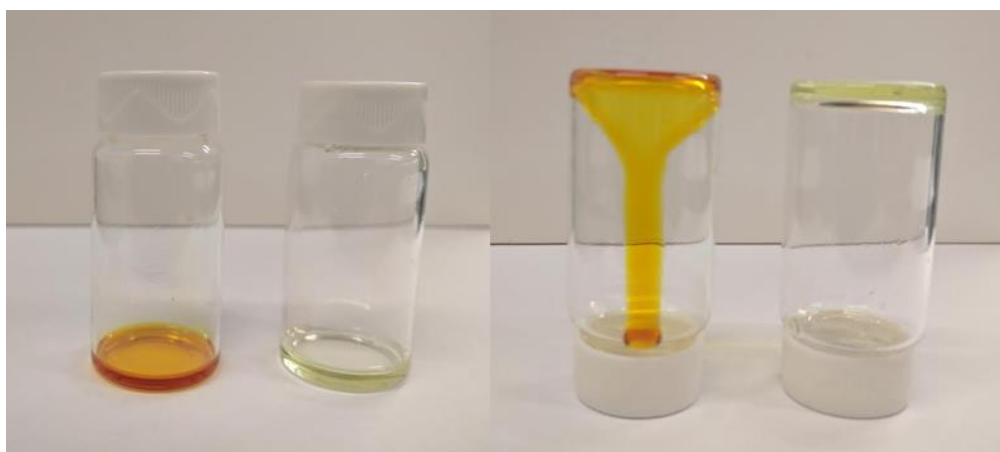


**Figure A10.** Mass spectrum of  $[\text{Gd(III)(hfacac)}_4]^-$  using TOF LC/MS (negative mode).

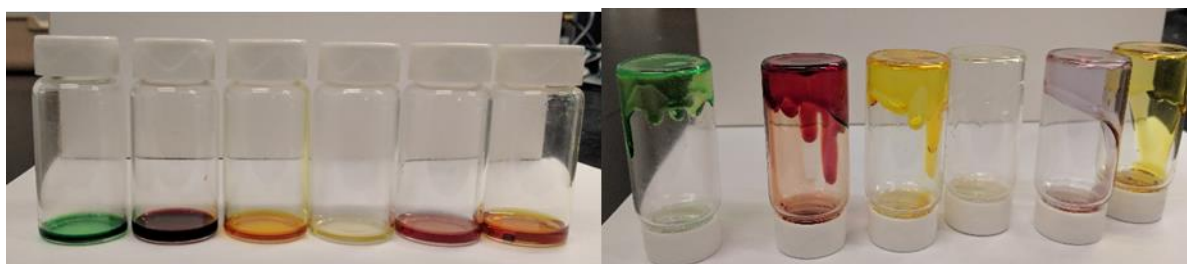




**Figure A11.** Mass spectrum of  $[\text{Nd(III)(hfacac)}_4]^-$  using TOF LC/MS (negative mode).



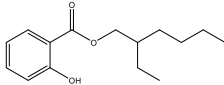
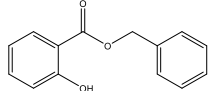
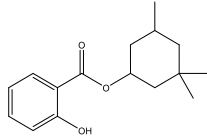
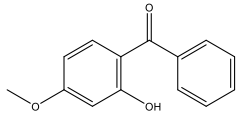
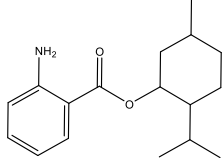
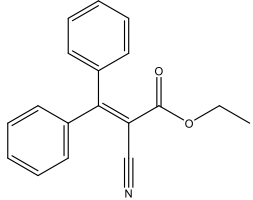
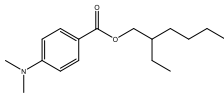
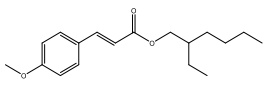
**Figure A12.**  $[\text{P}_{66614}^+][\text{Mn(II)(hfacac)}_3^-]$  (left) and  $[\text{P}_{66614}^+]_2[\text{MnCl}_4^{2-}]$  (right) before and after inversion for 2 seconds.



**Figure A13.** From left to right:  $[\text{P}_{66614}^+][\text{Ni(II)(hfacac)}_3^-]$ ,  $[\text{P}_{66614}^+][\text{Co(II)(hfacac)}_3^-]$ ,  $[\text{P}_{66614}^+][\text{Mn(II)(hfacac)}_3^-]$ ,  $[\text{P}_{66614}^+][\text{Dy(III)(hfacac)}_4^-]$ ,  $[\text{P}_{66614}^+][\text{Nd(III)(hfacac)}_4^-]$ , and  $[\text{P}_{66614}^+][\text{Gd(III)(hfacac)}_4^-]$  before and after inversion for 1 second.

**APPENDIX B**  
**SUPPLEMENTAL INFORMATION ACCOMPANYING**  
**CHAPTER 3**

**Table B1.** Chemical structures, retention time, quantifier and qualifier ions utilized for the identification and quantification of the target UV filters in the HS-GC-MS system. The segment program utilized in the MS during the single ion monitoring (SIM) acquisition is also included.

Analyte	Structure	Retention time (min)	Quantifier ion (m/z)	Qualifier ion (m/z)	Segment	Time (min)	Registered ions
ES		7.858	120	138	1: ES	7.85	120, 138
BS		8.205	91	65	2: BS	8.18	65, 91
HS		8.270	138	109	3: HS	8.23	109, 138
BP3		8.896	151	77	4: BP3	8.85	77, 151
MA		9.239	137	119	5: MA	9.20	119, 137
ETO		9.471	232	204	6: ETO	9.42	204, 232
EPP		9.827	165	148	7: EPP	9.80	148, 165
EMC		10.00	178	161	8: EMC	9.96	161, 178

\*Grey rows denote segments in the SIM acquisition program

**Table B2.** Volumes of IL and LiNTf<sub>2</sub> solution needed to produce approximately 25  $\mu\text{L}$  of sedimented IL for *in situ* DLLME analysis of UV filters from 5 mL of aqueous solution.

IL applied for <i>in situ</i> DLLME	Volume of the IL solution added ( $\mu\text{L}$ ) <sup>a</sup>	Volume of the LiNTf <sub>2</sub> solution added ( $\mu\text{L}$ ) <sup>b</sup>
[BMIM <sup>+</sup> ][Br <sup>-</sup> ]	250	164 <sup>c</sup> 246 <sup>d</sup>
[OMIM <sup>+</sup> ][Br <sup>-</sup> ]	150	78 <sup>c</sup> 119 <sup>d</sup>
[BeBIM <sup>+</sup> ][Br <sup>-</sup> ]	180	88 <sup>c</sup> 132 <sup>d</sup>
[BeEOHIM <sup>+</sup> ][Br <sup>-</sup> ]	350	188 <sup>c</sup> 266 <sup>d</sup>
[HeOHMIM <sup>+</sup> ][Cl <sup>-</sup> ]	360	236 <sup>c</sup> 354 <sup>d</sup>

<sup>a</sup> The IL solution was prepared by dissolving 2 g of IL in 10 mL of ultrapure water.

<sup>b</sup> The LiNTf<sub>2</sub> solution was prepared by dissolving 4 g of LiNTf<sub>2</sub> in 10 mL of ultrapure water.

<sup>c</sup> Molar ratio of IL:LiNTf<sub>2</sub>=1:1.

<sup>d</sup> Molar ratio of IL:LiNTf<sub>2</sub>=1:1.5.

**Table B3.** Comparison of the developed method to existing microextraction methods for determination of UV filters.

Microextraction method <sup>a</sup>	Instrumentation <sup>b</sup>	Extraction time (min)	Simultaneous extractions are possible	Number of simultaneous extractions	LOD (ng L <sup>-1</sup> )	Ref.
SPME	GC-MS	30–40	No	1	2.8-26	[1]
SPME	LC	60–75	No	1	100-5000	[2]
SBSD $\mu$ E	GC-MS	40	Yes	- <sup>c</sup>	13-148	[3]
SPME	GC-MS-MS	25	No	1	.068-12	[4]
<i>In situ</i> DLLME	HS-GC-MS	~7	Yes	6 <sup>d</sup>	500-5000	This work

<sup>a</sup> Solid-phase microextraction (SPME); Stir bar sorptive-dispersive microextraction (SBSD $\mu$ E); Dispersive liquid-liquid microextraction (DLLME)

<sup>b</sup> Gas chromatography (GC); mass spectrometry (MS); Liquid chromatography (LC); headspace (HS)

<sup>c</sup> Not studied

<sup>d</sup> The number of simultaneous extractions is limited by the capacity of the centrifuge

## References

- [1] M.J. Trujillo-Rodriguez, H. Nan, J.L. Anderson, J. Chromatogr. A 1540 (2018) 11
- [2] J. An, J.L. Anderson, Talanta 182 (2018) 74
- [3] J.L. Benede, A. Chisvert, D.L. Giokas, A. Salvador, Talanta 147 (2016) 246
- [4] M. Vila, M. Celeiro, J.P. Lamas, T. Dagnac, Anal. Methods 8 (2016) 70

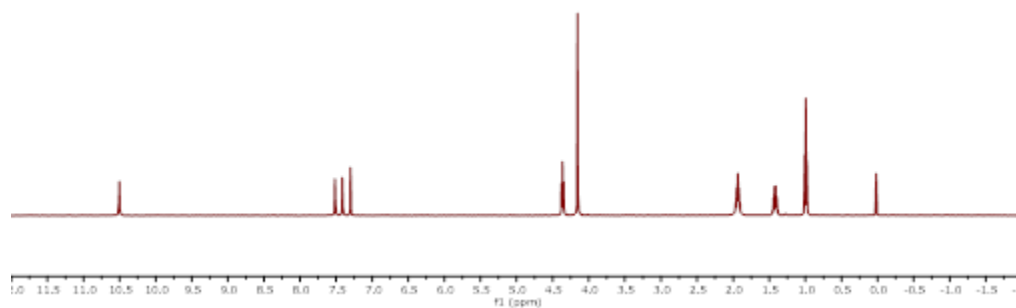


**Figure B1.**  $^1\text{H-NMR}$  (500 MHz, Chloroform-*d*) spectrum of  $[\text{BMIM}^+][\text{Br}^-]$ : 10.46 (s, 1H), 7.47 (t,  $J = 1.8$  Hz, 1H), 7.37 (t,  $J = 1.8$  Hz, 1H), 4.32 (t,  $J = 7.4$  Hz, 2H), 4.12 (s, 3H), 1.95-1.84 (m, 2H), 1.42-1.32 (m, 2H), 0.95 (t,  $J = 7.4$  Hz, 3H).

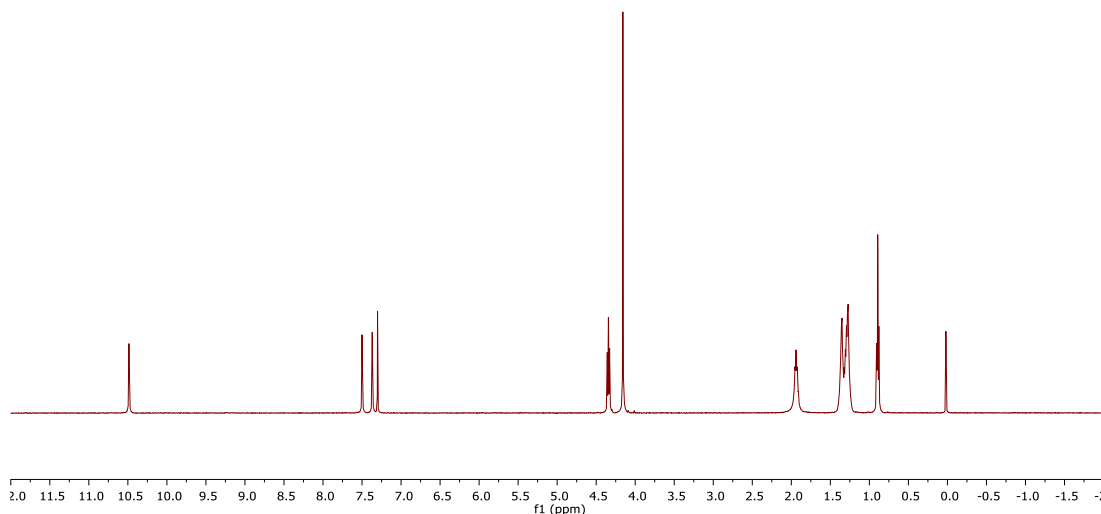


**Figure B2.**  $^1\text{H-NMR}$  (500 MHz, Chloroform-*d*) spectrum of  $[\text{OMIM}^+][\text{Br}^-]$ : 10.45 (s, 1H), 7.46 (t,  $J = 1.8$  Hz, 1H), 7.33 (t,  $J = 1.8$  Hz, 1H), 4.30 (t,  $J = 7.5$  Hz, 2H), 4.12 (s, 3H), 1.95-1.84 (m, 2H), 1.37 - 1.18 (m, 10H), 1.85 (t,  $J = 6.8$  Hz, 3H).

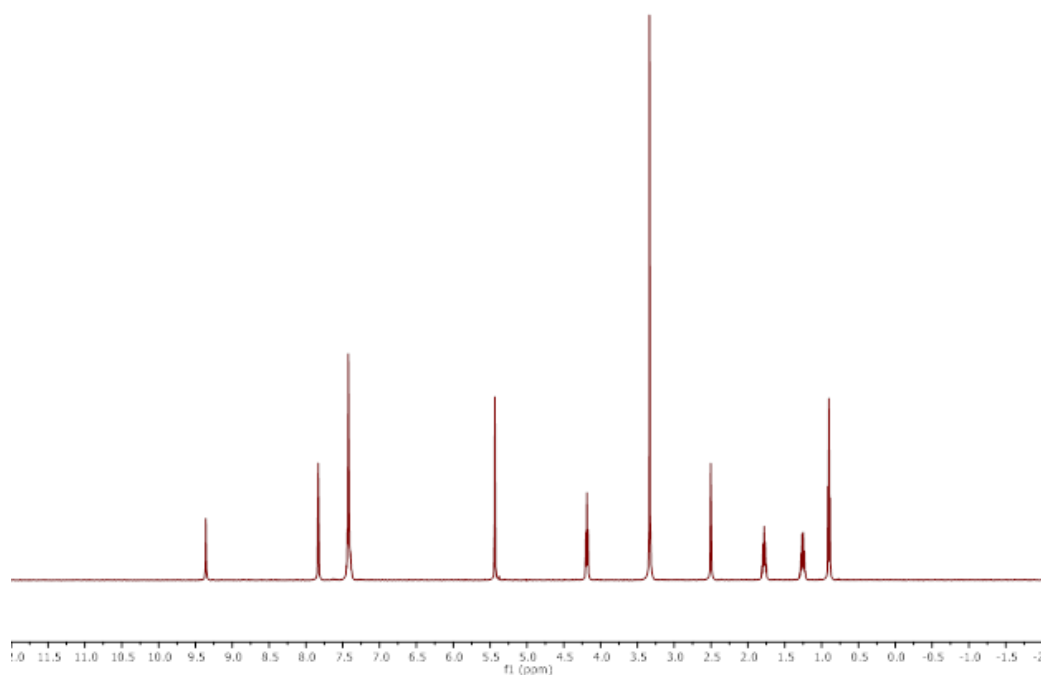


**Figure B3.**  $^1\text{H-NMR}$  (500 MHz,  $\text{DMSO-}d_6$ ) spectrum of  $[\text{BeBIM}^+][\text{Br}^-]$ : 9.35 (s, 1H), 7.83 (d,  $J = 1.7$  Hz, 2H), 7.47-7.36 (m, 5H), 5.43 (s, 2H), 4.18 (t,  $J = 7.2$  Hz, 2H), 1.83-1.72 (m, 2H), 1.31-1.20 (m, 2H), 0.9 (t,  $J = 7.4$  Hz, 3H).

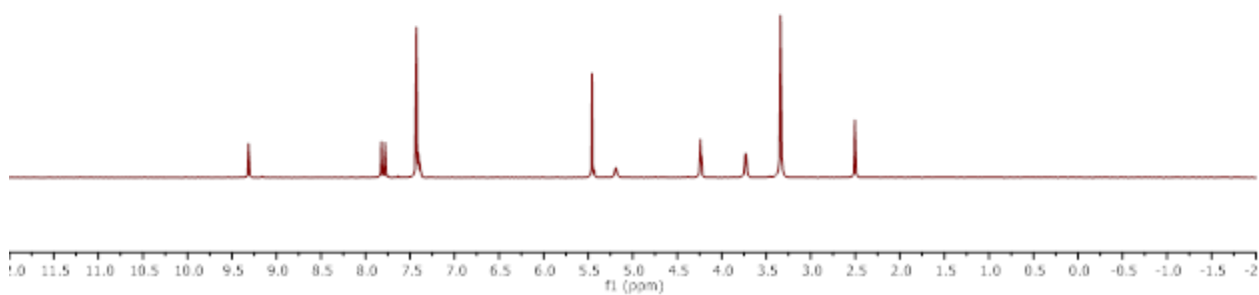


**Figure B4.**  $^1\text{H-NMR}$  (500 MHz,  $\text{DMSO-}d_6$ ) spectrum of  $[\text{BeEOHIM}^+][\text{Br}^-]$ : 9.31 (s, 1H), 7.82 (t,  $J = 1.8$  Hz, 1H), 7.78 (t,  $J = 1.8$  Hz, 1H), 7.46-7.37 (m, 5H), 5.45 (s, 2H), 5.20 (br. s., 1H), 4.24 (t,  $J = 5.0$  Hz, 2H), 3.73 (t,  $J = 4.0$  Hz, 2H).

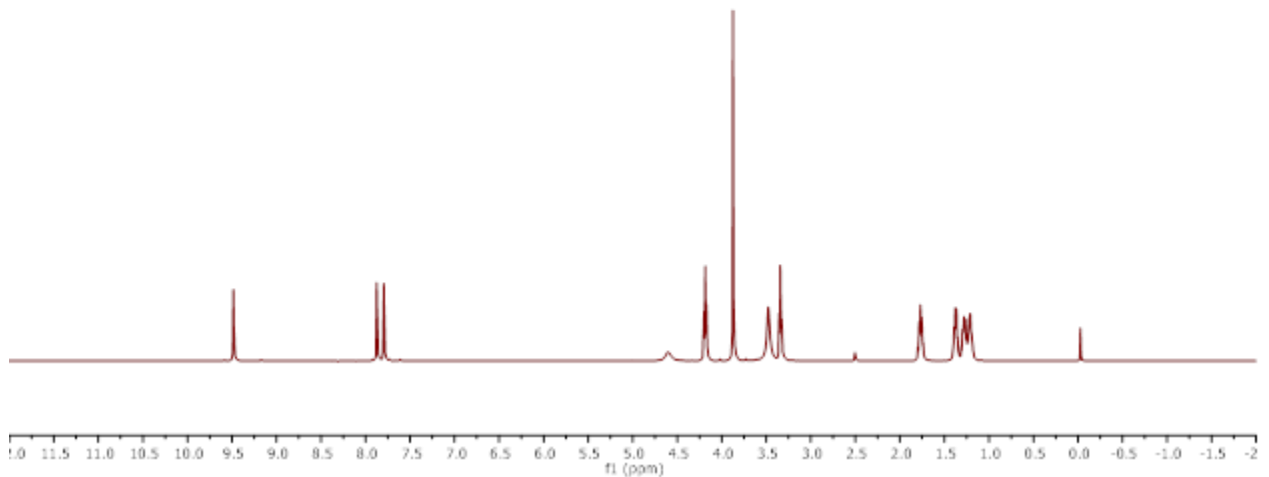


**Figure B5.**  $^1\text{H-NMR}$  (500 MHz,  $\text{DMSO-}d_6$ ) spectrum of  $[\text{HeOHMIM}^+][\text{Cl}^-]$ : 9.28 (s, 1H), 7.81 (t,  $J = 1.8$  Hz, 1H), 7.73 (t,  $J = 1.8$  Hz, 1H), 4.61 (br. s., 1H), 4.16 (t,  $J = 7.2$  Hz, 2H), 3.86 (s, 3H), 3.36 (t,  $J = 5.7$  Hz, 2H), 1.77 (td,  $J = 7.5, 14.8$  Hz, 2H), 1.44 - 1.35 (m, 2H), 1.33 - 1.25 (m, 2H), 1.25 - 1.17 (m, 2H)

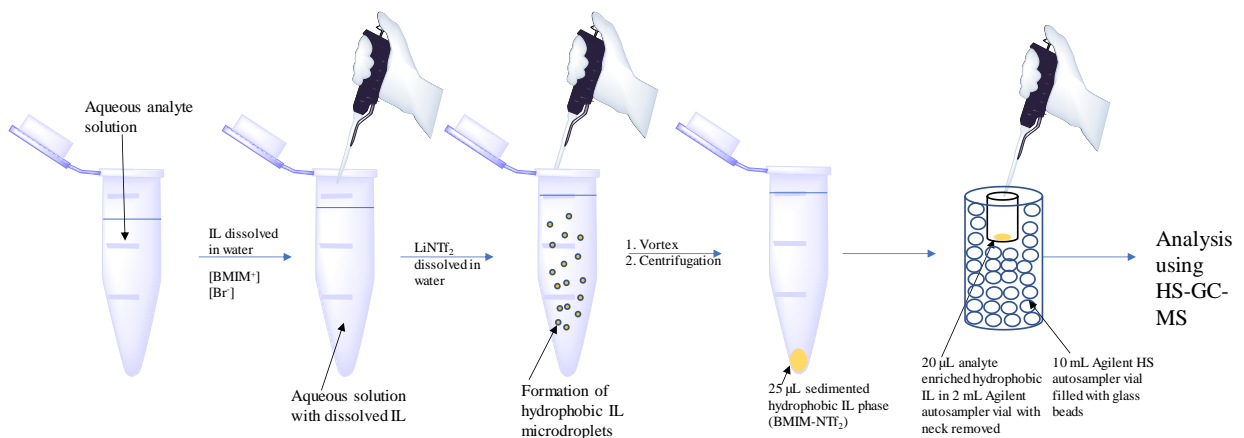


**Figure B6.** Graphical representation of the *in situ* DLLME procedure and the reduced volume headspace system.

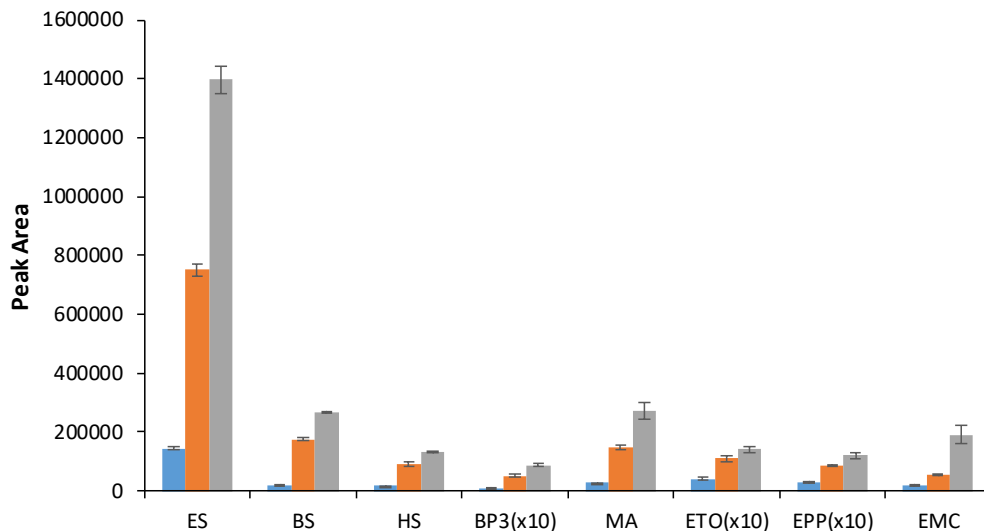


**Figure B7.** Effect of total sample volume on the extraction efficiencies (expressed in peak area) of UV filters from (■) 2.5 mL, (■) 5 mL, and (■) 10 mL of ultrapure water. [BMIM<sup>+</sup>][Br<sup>-</sup>] volume: 20  $\mu$ L; headspace incubation temperature: 200  $^{\circ}$ C; IL:NTf<sub>2</sub> = 1:1; Concentration of analytes ETO and EPP: 1 mg L<sup>-1</sup>; Concentration of the remaining analytes: 200  $\mu$ g L<sup>-1</sup>; Vortex time: 10 s.

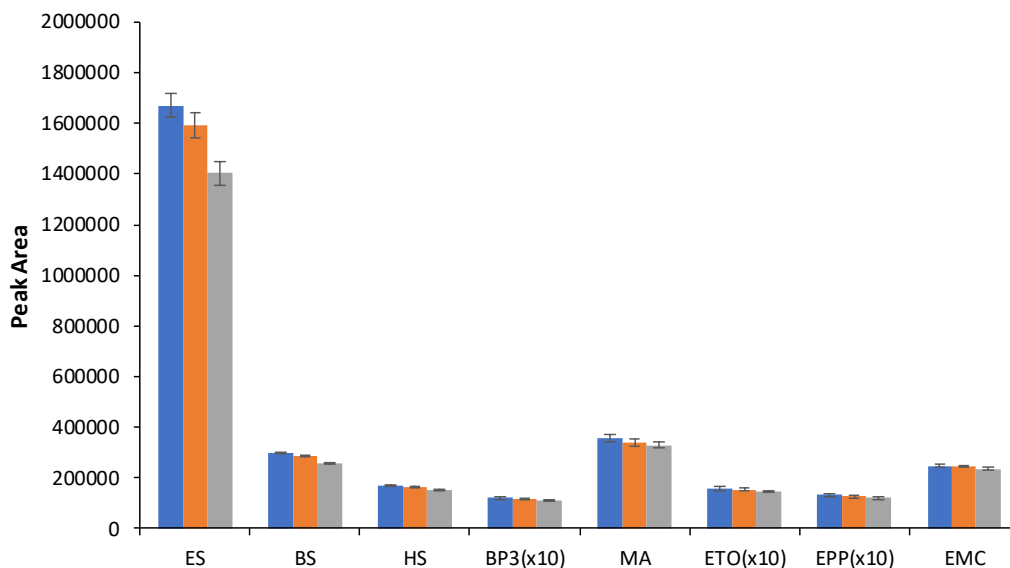


**Figure B8.** Effect of NaCl concentration on extraction efficiencies (expressed in peak area) of UV filters from 10 mL total sample volume at (■) 0% NaCl (w/v), (■) 3.5% NaCl (w/v), and (■) 5% NaCl (w/v). [BMIM<sup>+</sup>][Br<sup>-</sup>] volume: 20  $\mu$ L; IL:NTf<sub>2</sub> = 1:1; Headspace incubation temperature: 200  $^{\circ}$ C; Concentration of analytes ETO and EPP: 1 mg L<sup>-1</sup>; Concentration of the remaining analytes: 200  $\mu$ g L<sup>-1</sup>; Vortex time: 30 s.



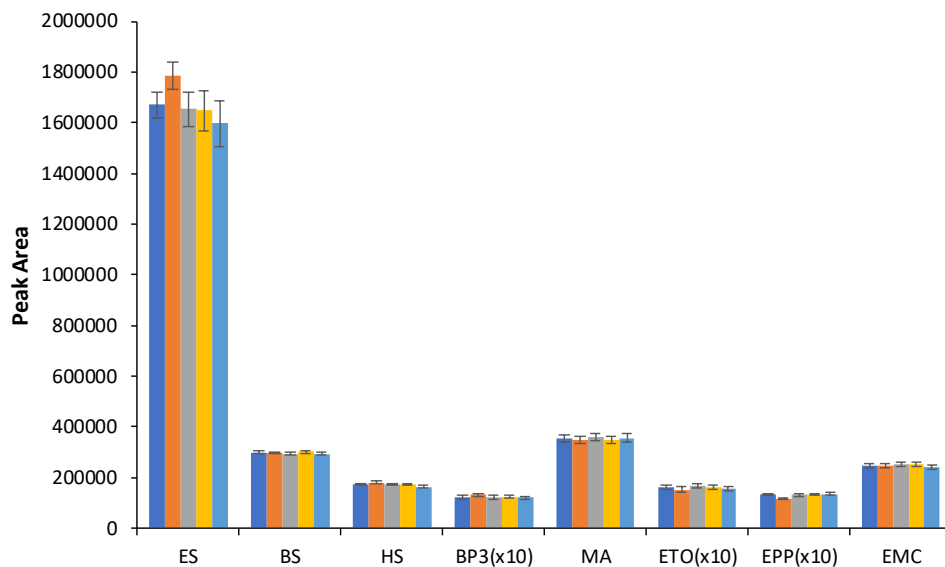


**Figure B9.** Effect of pH on extraction efficiencies (expressed in peak area) of UV filters from 10 mL total sample volume. (■) ultrapure water, (■) pH 4, (■) pH 6, (■) pH 8, and (■) pH 10. [BMIM<sup>+</sup>][Br<sup>-</sup>] volume: 20  $\mu$ L; IL:NTf<sub>2</sub> = 1:1; Headspace incubation temperature: 200 °C; Concentration of analytes ETO and EPP: 1 mg L<sup>-1</sup>; Concentration of the remaining analytes: 200  $\mu$ g L<sup>-1</sup>; Vortex time: 30 s.